Vol. 15: 161–183, 2000 | CLIMATE RESEARCH Clim Res | Published September 5

A model analysis of the relationship between climate perturbations and carbon budget anomalies in global terrestrial ecosystems: 1970 to 1997

Akihiko Ito*, Takehisa Oikawa

Institute of Biological Sciences, University of Tsukuba, Tennodai 1-1-1, Tsukuba, Ibaraki 305-8572, Japan

ABSTRACT: We performed a model analysis of the effect of climatic perturbations from 1970 to 1997 on the carbon budget of terrestrial ecosystems at the global scale. The model, Sim-CYCLE, enabled us to simulate carbon storage in terrestrial pools and monthly carbon fluxes between the atmosphere and the biosphere, e.g. photosynthesis, respiration, decomposition, and net ecosystem production (NEP). For the global analysis, we adopted the Matthews biome distribution map (12 biome types) and the US National Centers for Environmental Prediction and the US National Center for Atmospheric Research (NCEP/NCAR) reanalysis climate dataset, which is at a spatial resolution of T62 (5828 land cells). During the 28 yr experimental period, global NEP showed considerable climate-induced interannual anomalies (ΔNEPs) ranging from –2.06 Pg C yr^{-1} (source) in 1983 to +2.25 (sink) Pg C yr^{-1} in 1971, being sufficiently large to give rise to anomalies in the atmospheric CO_2 concentration from +0.97 to –1.06 ppmv. Regression analyses demonstrated the following: (1) annual ΔNEPs had the highest correlation ($r^2 = 0.38$) with the temperature anomaly at the global scale; (2) the anomalies in precipitation resulted in a considerable ΔNEP in northern high and middle regions; (3) an anomalous global warming by +1°C brought about a negative ΔNEP of –2.7 Pg C yr^{-1}; (4) the responsiveness was primarily attributable to the temperature sensitivities of plant respiration and soil decomposition, and secondarily to the moisture sensitivity of decomposition; and (5) the temperature dependence of ΔNEP had a clear seasonality, i.e. most sensitive in July to September (summer in the northern hemisphere) relative to other seasons. In 1983, when an ENSO event happened and the tropical zone was anomalously hot (0.4°C above the long-term mean), the largest negative ΔNEP (–2.06 Pg C yr^{-1}) was estimated. On the other hand, in 1971, when global mean temperature was relatively low (0.2°C below the long-term mean), the largest positive ΔNEP (+2.25 Pg C yr^{-1}) was estimated. Furthermore, in 1992, when an anomalous cooling during the growing period (0.3°C below the long-term mean) was caused by the Mt. Pinatubo eruption (June 1991), a considerable positive ΔNEP (+1.14 Pg C yr^{-1}) was estimated. The climate dependencies of global terrestrial ecosystems analyzed here may contain significant implications not only for the present functioning of atmosphere-biosphere carbon exchange, but also for ongoing global warming.

KEY WORDS: Carbon budget · Terrestrial ecosystem · Net ecosystem production (NEP) · Interannual change · Climatic perturbation · Model analysis

1. INTRODUCTION

Terrestrial ecosystems play a critical role in the global carbon cycle (Bolin et al. 1979). However, in spite of a large amount of effort, we can only roughly quantify the extent of the terrestrial ecosystem net carbon sink, and how it will change in the future. We should take 3 major effects into account at the global scale: the ongoing CO_2 enrichment, climate change, and human land-use change. Anthropogenic CO_2 emission has steadily increased the atmospheric CO_2 concentration since the pre-industrial revolution age; this rising concentration has exerted a monotonous, although non-linear, fertilization effect on the ecosystem carbon cycle (Melillo et al. 1996). Human land-use

*E-mail: itoh@oak.biol.tsukuba.ac.jp

change may be the most complicated factor to predict, but qualitatively this effect has reduced and will continue to reduce carbon storage of the biosphere (Houghton et al. 1998). In comparison, the impacts of climate change on the biosphere, even their direction, are less clear for the following reasons: (1) climate influences various ecosystem processes simultaneously; (2) a number of climatic factors, such as temperature, precipitation, and irradiance, change concurrently and affect ecosystem processes interactively; (3) spatial variability of climatic anomalies is large and scale dependent; and (4) several fluctuations that have different time-scales are multiplicatively combined in the observed climate records.

In this study, we put emphasis on the effect of interannual climatic perturbations, so that we may address the environmental dependency of the atmosphere-biosphere CO_2 exchange. An El Niño/Southern Oscillation (ENSO) event represents the most obvious interannual climate change, and often is accompanied by regionally warmer temperatures and lower precipitation (Ropelewski & Halpert 1987, Halpert & Ropelewski 1992). Also, a huge volcanic eruption can lead to attenuated direct solar radiation and cooler surface temperatures (Robock & Mao 1995). These clear perturbations may have an influence on ecosystem productivity at the broad scale, as observed by remote sensing (Myneni et al. 1997).

The short-term impact of climate change on ecosystems should be mainly regulated by a couple of physiological processes, and then we can describe the impacts with an ecophysiology-based model. Although the atmosphere-biosphere CO_2 exchange is partly affected by such disturbance processes as fire and deforestation, we focus only on those processes regulated at the physiological level, such as photosynthesis, respiration, and decomposition. Other processes, in particular biomass burning, may provide a substantial contribution not only at the local scale but also at the continental scale, and they have been addressed by other studies (e.g. Wittenberg et al. 1998).

In this paper, we simulate the time-series of atmosphere-biosphere CO_2 exchange for 1970 to 1997, and analyze the relationship between the climate perturbations and the anomalies in the terrestrial carbon budget, especially in net ecosystem production (ΔNEP), which indicates whether an ecosystem acted as a net carbon sink or a source during a given period. Then, we discuss whether the estimated ΔNEP could have an influence to such an extent that it contributed to the observed anomalies in the atmospheric CO_2 concentration (Keeling et al. 1995). Indeed, this issue has attracted the attention of researchers of global carbon cycle models (e.g. Dai & Fung 1993, Kaduk & Heimann 1994, Maisongrande et al. 1995, Kindermann et al. 1996, Gérard et al. 1999, Potter et al. 1999, Rayner & Law 1999). We employ a process-based carbon cycle model of terrestrial ecosystems (Sim-CYCLE) to simulate the carbon budget.

2. CLIMATE DATASET

The climate condition for the model analysis is derived from the reanalysis dataset produced by the US National Centers for Environmental Prediction and the US National Center for Atmospheric Research (NCEP/NCAR). This is a gridded dataset in which observation records were interpolated by the 4-dimensional data assimilation method (Kalnay et al. 1996). At this stage, the monthly composite dataset is available for 28 yr, from January 1970 to December 1997; we took this interval to be the experimental period. In the NCEP/NCAR-reanalysis dataset, surface variables are arranged on a Gaussian grid of T62 resolution (94×192 grid cells, latitude and longitude), which seems likely to be sufficiently fine for the purpose of global analysis; we took this resolution to be the spatial resolution of simulation in this research. The carbon budget was calculated autonomously for each of the 5828 terrestrial grid points.

The advantage of adopting the reanalysis dataset is, we postulate, due to the climatological consistency and homogeneous accuracy throughout the experimental period. In addition, the NCEP/NCAR-reanalysis dataset provides a larger number of diagnostic variables than those datasets derived from simple interpolation of observations (e.g. Leemans & Cramer 1991, New et al. 1999). The following variables were adopted for our model analysis: surface downward shortwave radiation fluxes (SWR, in W m^{-2}); ground surface air temperature (TG, in °C); soil temperatures at 10 and 200 cm depth (TS_{10} and TS_{200}, in °C); potential evapotranspiration rate (PET, in W m^{-2}); latent heat flux (i.e. actual evapotranspiration rate, AET, in W m^{-2}); and volumetric soil moisture contents at 10 and 200 cm depth (SMC_{10} and SMC_{200}, as a fraction). Additionally, the monthly precipitation (PR, in mm mo^{-1}), although not a model input, was used later in the regression analysis between the simulation outcome and climatic factors.

Because plant CO_2 assimilation utilizes only photosynthetically active radiation (PAR; 400 to 700 nm) in the spectrum of total SWR, the surface irradiance (PAR_{SFC}; µmol photon m^{-2} s^{-1}) is given by the following:

$$PAR_{SFC} = 4.2 \cdot (SWR \cdot 0.45) \quad (1)$$

where multipliers 4.2 and 0.45 are for unit conversion from W m^{-2} to µmol photon m^{-2} s^{-1}, and for extraction of the fraction of PAR, respectively (Larcher 1995).

A climatic anomaly is defined as the difference from the 28 yr average value, and was used for linear and multiple regression analyses with the carbon flux anomalies. Before the multiple regression analysis, mutual correlations among the climatic components were checked to specify a combination of independent variables.

3. OVERVIEW OF CARBON CYCLE MODEL

A process-based model has been developed for simulating the carbon dynamics of terrestrial ecosystems at the global scale. The basis of the model is on the dry-matter production theory established by Monsi & Saeki (1953); Oikawa (1985) constructed a theory-based ecosystem model, which successfully retrieved growth and succession in tropical forest (Oikawa 1985), temperate forest (Oikawa 1998), and grassland (Oikawa 1995) ecosystems. In this study, the ecosystem-scale model was extended to a global-scale model, and termed Sim-CYCLE (Simulation model of Carbon cYCle in Land Ecosystems). The model conceptualizes the terrestrial carbon dynamics as a 5-compartment system (Fig. 1): foliage, stem and branch, root, litter (dead biomass), and mineral soil. The model's carbon fluxes were gross primary production (GPP), plant autotrophic respiration (AR), litterfall, translocation, and heterotrophic respiration from the decomposing soil organic matter (HR). All the carbon fluxes were calculated monthly. In terms of the carbon budget, net primary production (NPP) and net ecosystem production (NEP) are critically important, because NPP (= GPP – AR) represents the biological productivity supporting all ecosystem structures and functions, and NEP (= NPP – HR) dictates the net balance with the atmospheric CO_2. For example, NEP is positive when acting as a net sink. The ecophysiological parameters in model formulae were successfully calibrated so that the model agreed sufficiently with field observations.

The biome distribution for the global simulation was derived from the mapping by Matthews (1983), for both potential biome and cultivation intensity. In our model analysis (Table 1), the spatial resolution of the original dataset, i.e. 1-degree latitude-longitude, was adjusted to that of the NCEP/NCAR-reanalysis by resampling the grid points, and the natural biome categories, i.e. 32 original types, were simplified into 12 types. From the cultivation intensity in the dataset, we can estimate the general extent of the human land-use change, although we did not include the additional deforestation during the experimental period. In arid rangelands, including savanna, grassland, and desert (biomes 7, 8, and 11 in Table 1), calculation of C_3 and C_4 plants is separately carried out because of their significant differences in photosynthetic capacity and sensitivities to temperature, aridity, and CO_2 conditions. The ecophysiological discrepancies between C_3 and C_4 species are reflected in their geographical distribution (C_4 species have larger predominance in lower and warmer latitudes), and may have notable

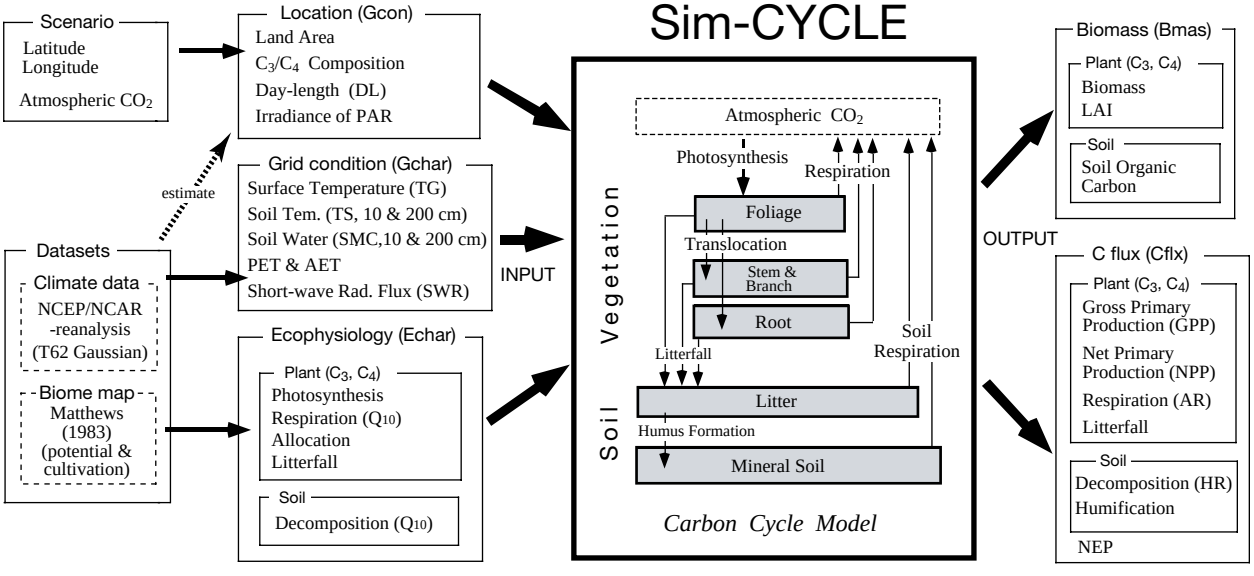

Fig. 1. Schematic of the simulation model Sim-CYCLE, in which the terrestrial carbon cycle is conceptualized by a 5-compartment system. The model, coded in the programming language C, has 3 input structures (Gcon, Gchar, and Echar) and 2 output structures (Bmas and Cflx) (the term 'structure' means assemblage of variables in C). The environmental conditions used in this paper are also shown. PAR: photosynthetically active radiation; PET, AET: potential and actual evapotranspiration rates; LAI: leaf area index; AR, HR: auto- and heterotrophic respiration

Table 1. Biome types used for the model analysis, and their area and frequency in the T62 Gaussian grid scale. Original data are after Matthews (1983), including the potential biome and the cultivation intensity for each grid point. Areas of natural-vegetation are listed in 5 latitudinal zones (Z1 to Z5). Values in **bold**: the distribution center that has the largest area for each biome; underlined values: the most dominant biome for each latitudinal zone

Biome		Z1 90–50° N	Z2 50–20° N	Z3 20° N–20° S	Z4 20–50° S	Z5 50–90° S	Total Natural	Total Cultivated	Frequency (cells)
		(10^6 km^2)							
1	Tropical evergreen forest	0.0	0.0	**11.9**	0.4	0.0	12.3	0.3	287
2	Tropical seasonal forest	0.0	**3.2**	2.4	1.2	0.0	6.8	1.9	211
3	Temperate broad-leaved evergreen forest	0.0	**1.0**	0.0	0.4	0.0	1.4	0.5	51
4	Temperate deciduous forest	**7.9**	1.9	0.0	0.0	0.0	9.8	4.1	526
5	Temperate and boreal needle-leaved forest	**5.5**	4.6	0.6	0.5	0.1	11.2	0.5	424
6	Woodland	**4.3**	0.7	1.5	0.9	0.0	7.5	0.4	318
7	Savanna	0.0	0.2	**3.8**	0.1	0.0	4.0	1.0	117
8	Grassland	2.1	9.4	**10.4**	5.4	0.1	27.3	6.2	918
9	Shrub	0.7	**5.3**	1.9	4.0	0.1	12.0	0.8	367
10	Tundra	**6.5**	0.0	0.0	0.0	0.0	6.5	0.0	370
11	Desert	0.3	**11.5**	1.6	1.1	0.0	14.5	0.3	401
12	Ice sheet	2.4	0.0	0.0	0.0	**12.1**	14.5	0.0	1838
	Land total	29.8	37.7	34.0	13.9	12.4	127.7	16.0	5828

importance under global change conditions (Collatz et al. 1998). The C_3/C_4 composition in arid rangeland grids was empirically estimated by a regression model relating the composition with latitude (e.g. review by Sage et al. 1999, see also Teeri & Stowe 1976, Ehleringer et al. 1997).

For each grid point, simulation began from a juvenile stage of the ecosystem with little carbon storage (0.1 Mg C ha^{-1} for each compartment), and through the iterative calculation (over 4000 yr) the carbon budget was to be fully stabilized so as to reach the climax stage, where annual NEP is equal to zero. In addition, in cultivated areas, a typical cultivation cycle from spring planting to autumn harvesting was modelled. The calculations were performed under a stationary atmospheric CO_2 level: 325.5 ppmv, that is, the background level in 1970 (World Data Centre for Greenhouse Gases [WDCGG 1998]). Consequently, we obtained the equilibrium carbon budget both in natural and in agricultural ecosystems at the beginning of the simulation; this made it tractable to analyze the interannual change in the terrestrial carbon budget.

After that, the real simulation from 1970 to 1997 was carried out using the actual climatic and atmospheric CO_2 conditions. During the experimental period, the atmospheric CO_2 concentration increased at the rate of approximately +1.4 ppmv yr^{-1}, from 325.5 to 364.5 ppmv (WDCGG 1998). Note that we focused on the effect of climate perturbations, although the actual and modeled ecosystem carbon dynamics are sensitive to the atmospheric CO_2 level. Exploring the effects of CO_2 fertilization on the global carbon cycle remains to be done in our future research. Then, to remove the trend induced by the CO_2 fertilization effect from the bulk trend (see Fig. 9A), we performed a supplementary simulation using the actual CO_2 increase and the average stationary climate condition (see Fig. 9B).

$$\Delta F_{bulk} = F_{bulk} - \overline{F_{bulk}} \quad (2a)$$

$$\Delta F_{CO_2} = F_{CO_2} - \overline{F_{CO_2}} \quad (2b)$$

where F represents GPP, AR, NPP, HR, or NEP. F_{bulk} and F_{CO_2} denote the carbon fluxes calculated by simulations using the actual and average climate data, respectively (the line over these variables indicates the 28 yr arithmetic mean). By comparing these 2 trends, we clarified the climate-induced short-term anomalies in terrestrial carbon flux ΔF (see Fig. 9C), which takes the form:

$$\Delta F = \Delta F_{bulk} - \Delta F_{CO_2} \quad (2c)$$

Most of the analyses in this paper deal with this carbon flux anomaly.

Modelling of the environmental dependencies is a critical point for the simulation research of carbon exchange processes. Thus, Sim-CYCLE incorporates the environmental dependencies on the basis of physiological responses, i.e. at the scale of organs such as a single leaf, where a large amount of observations and experiments have been accumulated. In the next section, we present brief descriptions of carbon fluxes and their dependencies on light, temperature, and water conditions. The physiological regulation is first described, and scaling-up to the ecosystem-level regulation of the carbon budget is then covered. Several representative parameters are shown in Table 2.

Table 2. Ecophysiological parameters in Sim-CYCLE. PC_{MAX}: maximum photosynthetic rate (μmol CO_2 m^{-2} s^{-1}); KA: light attenuation coefficient (dimensionless); T_{MIN}, T_{OPT}, and T_{MAX}: minimum, optimum, and maximum temperatures for photosynthesis, respectively (°C); GS_{MAX}: maximum stomatal conductance (μmol CO_2 m^{-2} s^{-1}); KM_{GS}: coefficient of stomatal conductance (μmol CO_2 m^{-2} s^{-1}); $SARM_{(TG=15°C)}$: specific maintenance respiration rate for each organ at 15°C (Mg C Mg C^{-1} d^{-1}); and $SHR_{(TS=15°C)}$: specific heterotrophic respiration rate for each soil compartment at 15°C soil temperature (Mg C Mg C^{-1} d^{-1})

Biome		PC_{MAX}	KA	T_{MIN}	T_{OPT}	T_{MAX}	GS_{MAX}	KM_{GS}	$SARM_{(TG=15°C)}$			$SHR_{(TS=15°C)}$	
									Leaf	Stem	Root	Litter	Humus
1		23	0.60	3	25	45	200	30	0.25	0.019	0.065	0.047	0.025
2		25	0.60	3	25	45	200	25	0.23	0.009	0.042	0.043	0.031
3		18	0.55	0	22	38	190	30	0.34	0.022	0.085	0.042	0.026
4		21	0.50	−1	20	38	190	30	0.31	0.019	0.045	0.047	0.026
5		21	0.50	−4	20	38	190	30	0.30	0.008	0.025	0.049	0.032
6		21	0.48	−4	22	42	150	20	0.44	0.034	0.270	0.040	0.031
7	C_3	19	0.47	−2	25	45	140	20	0.52	0.062	0.340	0.037	0.028
	C_4	28	0.44	6	35	55	210	20	0.56	0.230	0.440	0.037	0.028
8	C_3	19	0.45	−2	22	45	140	20	0.53	0.068	0.340	0.042	0.031
	C_4	30	0.43	6	34	55	230	20	0.56	0.230	0.440	0.042	0.031
9		20	0.51	−2	25	45	140	20	0.51	0.025	0.290	0.038	0.032
10		19	0.47	−5	20	40	180	30	0.32	0.034	0.290	0.027	0.012
11		19	0.48	−3	26	44	150	15	0.50	0.059	0.270	0.063	0.055
Cultivated		24	0.48	−3	23	42	200	20	0.29	0.050	0.220	0.050	0.037

4. ENVIRONMENTAL DEPENDENCE

4.1. Light conditions. ***4.1.1. Single-leaf photosynthesis:*** Photosynthesis is the sole carbon exchange process dependent directly on light condition (Fig. 2). The single-leaf photosynthetic rate (PC in μmol CO_2 m^{-2} s^{-1}) is approximated by a rectangular hyperbolic equation of Michaelis-Menten type, as a function of the instantaneous irradiance (PAR_{INS}, μmol photon m^{-2} s^{-1}):

$$PC = \frac{PC_{SAT} \cdot LUE \cdot PAR_{INS}}{PC_{SAT} + LUE \cdot PAR_{INS}} \quad (3)$$

where PC_{SAT} is the light-saturated photosynthetic rate, and LUE is the light-use efficiency, or quantum yield of photosynthesis. In C_3 plants, the term LUE is a function of temperature and CO_2 conditions (0.04 to 0.06 mol CO_2 mol^{-1} photon), whereas in C_4 plants it is a constant (0.055 mol CO_2 mol^{-1} photon) (Ehleringer & Björkman 1977). However, for both C_3 and C_4 plants, the term PC_{SAT} is a function of temperature and CO_2 conditions, as described later. In general, PC of C_3 plants saturates to light below 1000 μmol photon m^{-2} s^{-1}, while that of C_4 plants is virtually free from light saturation. Under relatively weak irradiances, PC depends strongly on the irradiance, increasing linearly. On the other hand, during the growing period of vegetation, the daily maximum irradiance often exceeds 2000 μmol photon m^{-2} s^{-1}, and PC seems insensitive to small light fluctuations.

4.1.2 Gross photosynthetic production: The incident irradiance PAR_{INS} decreases vertically within the canopy (Monsi & Saeki 1953):

$$PAR_{INS} = PAR_{SFC} \cdot \exp(-KA \cdot LAI_c) \quad (4)$$

where PAR_{SFC} is the irradiance at the top of the canopy, KA is the attenuation coefficient (dimensionless) (Table 2), and LAI_c is the downward cumulative leaf area index from the top of the canopy (ha ha^{-1}). Furthermore, diurnal change in PAR_{SFC} is approximated by a sine-square function:

$$PAR_{SFC} = PAR_{MD} \cdot \sin^2(\pi \cdot t/DL) \quad (5)$$

where PAR_{MD} is the irradiance at midday, DL is the daylength (h), and t is the time from the dawn (h). Based on Eqs. (4) & (5), a multiple integral of Eq. (3) for ecosystem leaf area index (LAI, derived from leaf bio-

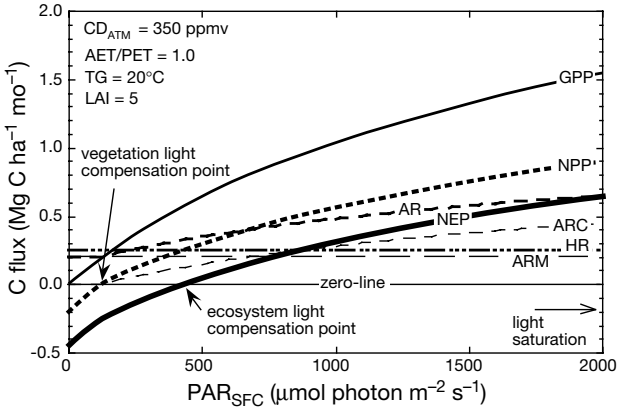

Fig. 2. Environmental responses of ecosystem carbon fluxes to irradiance of PAR_{SFC} (surface PAR). GPP, NPP: gross and net primary production; NEP: net ecosystem production; ARC, ARM: construction and maintenance respiration

mass [Mg C ha^{-1}] and specific leaf area [ha Mg^{-1} C]), and daylength gives a formula evaluating daily gross photosynthetic production (GPP in Mg C ha^{-1} d^{-1}) (Kuroiwa 1966):

$$\mathrm{GPP} = \frac{2\cdot\rho\cdot\mathrm{PC_{SAT}}\cdot\mathrm{DL}}{\mathrm{KA}} \cdot \ln\frac{1+\sqrt{1+\mathrm{KA}\cdot\mathrm{LUE}\cdot\mathrm{PAR_{MD}}/\mathrm{PC_{SAT}}}}{1+\sqrt{1+\mathrm{KA}\cdot\mathrm{LUE}\cdot\mathrm{PAR_{MD}}\cdot\exp(-\mathrm{KA}\cdot\mathrm{LAI})/\mathrm{PC_{SAT}}}} \quad (6)$$

where ρ (= 4.32×10^{-4}) is the conversion coefficient from µmol CO_2 m^{-2} s^{-1} to Mg C ha^{-1} d^{-1}. A monthly flux (Mg C ha^{-1} mo^{-1}) is calculated simply by multiplying the daily flux by the number of days in the month.

A large number of studies which addressed the relationship between irradiance and canopy-level production show that, generally, GPP needs a much stronger irradiance for light-saturation than single-leaf photosynthesis (see review by Ruimy et al. 1995). This suggests that canopy GPP is still sensitive to PAR_{SFC} during growing periods (Fig. 2). As well as for orbital factors, leading to seasonal and diurnal cycles, the surface irradiance may be influenced by cloudiness and atmospheric optical thickness, related to air dust and aerosol content.

4.2. Temperature condition. All of the atmosphere-biosphere CO_2 exchange processes are sensitive to temperature change in different fashions (Fig. 3).

4.2.1. Photosynthesis: The light-saturated leaf photosynthesis rate ($PC_{SAT} \geq 0$) varies with temperature, and is approximated by a bell-shaped function of ambient temperature TG (Raich et al. 1991) relative to the rate under the optimal temperature condition (PC_{OPT}):

$$\mathrm{PC_{SAT}(TG)} = \frac{(T_{MAX}-\mathrm{TG})(T_{MIN}-\mathrm{TG})}{(T_{MAX}-\mathrm{TG})(T_{MIN}-\mathrm{TG})-(T_{OPT}-\mathrm{TG})^2}\cdot\mathrm{PC_{OPT}} \quad (7)$$

where T_{MAX}, T_{MIN}, and T_{OPT} are the maximum, minimum, and optimum temperature (°C) for photosynthesis, respectively (Table 2). The LUE of C_3 plants is also a function of temperature (Ehleringer & Björkman 1977), given by the following expression:

$$\mathrm{LUE(TG)} = \mathrm{LUE_0}\cdot\frac{52-\mathrm{TG}}{3.5+0.75\,(52-\mathrm{TG})} \quad (8)$$

where LUE_0 is the constant value (= 0.055 mol CO_2 mol^{-1} photon). C_3 plants reduce their light-use efficiency with increasing temperature because of increased photorespiration, while C_4 plants are insensitive to temperature change. After upscaling to the canopy, or the temperature-GPP relationship (Fig. 3), it follows that the GPP is markedly insensitive to temperature fluctuation around T_{OPT}, but falls steeply near T_{MIN} and T_{MAX}. Temperature anomalies around the upper and lower temperature

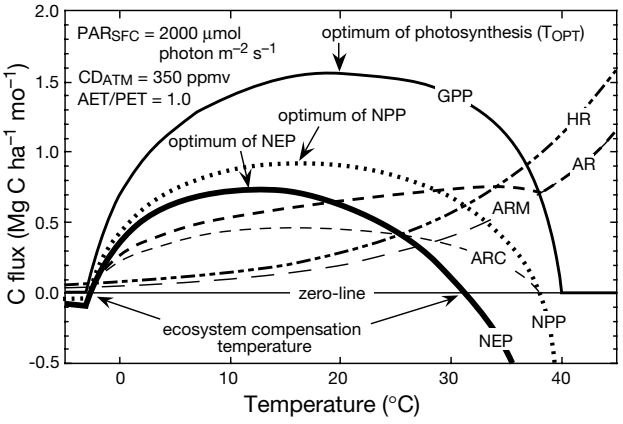

Fig. 3. Environmental responses of ecosystem carbon fluxes to temperature (TG for plant and TS for soil)

edges are important for another reason, that is, a warmer spring or autumn results in a longer growing-period, and cooler ones in a shorter growing period.

4.2.2. Plant autotrophic respiration: AR consists of 2 functional elements, the construction respiration (ARC) and the maintenance respiration (ARM). The term ARM is the cost to support a plant body and is proportional to biomass; its specific coefficient (SARM, in Mg C Mg^{-1} C d^{-1}) is an explicit function of temperature (control temperature 15°C):

$$\mathrm{SARM(TG)} = \mathrm{SARM_{(TG=15°C)}}\cdot\exp\left(\frac{\ln(Q_{10,ARM})}{10}(\mathrm{TG}-15)\right) \quad (9)$$

where $Q_{10,ARM}$ is the coefficient of temperature sensitivity, whose typical value is 2.0 (Ryan 1991). Thus, the rate AR respiration is directly and indirectly dependent on temperature, and generally increases when temperature rises. On the other hand, the term ARC is the cost of synthesizing new biomass and is proportional to the rate of growth; but, its specific coefficient (i.e. cost per unit biomass growth) is independent of environmental conditions (Amthor 1994). Note that the term ARC is related to the biomass growth rate, which is largely driven by GPP and is implicitly influenced by such environmental factors as irradiance, water availability, and ambient CO_2 level (see the correspondence between GPP and ARC in Fig. 3).

4.2.3. Soil decomposition: In spite of the paucity of information, HR is the crucial component in calculating NEP. The specific rate SHR is also an exponential function of soil temperature (TS in °C):

$$\mathrm{SHR(TS)} = \mathrm{SHR_{(TS=15°C)}}\cdot\exp\left(\frac{\ln(Q_{10,HR})}{10}\right)(\mathrm{TS}-15) \quad (10)$$

where TS is TS_{10} for the upper litter and TS_{200} for the lower mineral soil. The temperature sensitivity is

represented by the coefficient $Q_{10,HR}$ (Raich & Schlesinger 1992).

4.2.4. NPP and NEP: The sensitivity of NPP and NEP at the ecosystem level can be deduced from those of GPP, AR, and HR (Fig. 3). Fitter & Hay (1981) showed that the temperature NPP relationship is well described by a bell-shaped curve whose optimum temperature is lower than that of the temperature-GPP relationship (T_{OPT} of Eq. 7). The temperature-NEP relationship is also well described by a bell-shaped curve with an even lower optimum temperature than the NPP one. Actually, a warmer temperature accelerates evapotranspiration and reduces soil water content, and it may consequently affect plant production and soil decomposition (described next). This complexity resulting from the water-temperature interaction gives an additional motivation to adopt a process-based model, rather than an empirical model.

4.3. Water and CO_2 conditions. All of the atmosphere-biosphere CO_2 exchange processes are directly and indirectly sensitive to habitat water conditions, and many ecosystems suffer from chronic or periodic water deficit.

4.3.1. Photosynthesis: We assume that water availability primarily regulates the aperture of leaf stomata, through which plants exchange CO_2 and water simultaneously (Jones 1992). An empirical indicator, the ratio AET/PET, is derived directly from the NCEP/NCAR-reanalysis dataset. For example, as shown in Fig. 4, if the AET/PET ratio is nearly zero under a dry condition, leaf stomatal conductance (GS, in mmol CO_2 m^{-2} s^{-1}) is minimized so that plants do not lose water by transpiration. In contrast, if the AET/PET ratio is nearly unity, the soil is sufficiently wet and plants maximize stomatal conductance and CO_2 uptake. Under intermediate moisture conditions, stomatal aperture is estimated by linear interpolation between the maximum (AET/PET = 1) and minimum (AET/PET = 0) stomatal conductances (see Table 2 for GS_{MAX}). GS affects the intercellular CO_2 concentration (CD_{ICL}, in ppmv), estimated as follows:

$$CD_{ICL} = \frac{GS}{KM_{GS} + GS} CD_{ATM} \quad (11)$$

where KM_{GS} is the coefficient of stomatal conductance (mmol CO_2 m^{-2} s^{-1}), and CD_{ATM} is the atmospheric CO_2 concentration (ppmv). Eq. (11) shows how the atmospheric CO_2 concentration exerts a fertilization effect on plant photosynthesis. Finally, PC_{SAT} is parameterized as a function of CD_{ICL}:

$$PC_{SAT}(CD_{ICL}) = \frac{CD_{ICL}}{KM_{CD} + CD_{ICL}} PC_{MAX} \quad (12)$$

where PC_{MAX} is the photosynthetic rate under CO_2 saturation. The term KM_{CD} (ppmv) is the coefficient of CD_{INC} and represents the magnitude of the fertilization effect on photosynthetic rate. C_4 plants which are relatively insensitive to ambient CO_2 concentration have a low KM_{CD} value, whereas C_3 plants which augment productivity with increasing CO_2 level have a moderate to high one (Poorter 1993, Wullschleger 1995, Curtis & Wang 1998). Furthermore, intercellular CO_2 concentration affects the LUE of C_3 plants:

$$LUE(CD_{ICL}) = LUE_0 \frac{CD_{ICL}}{90 + 0.6 \cdot CD_{ICL}} \quad (13)$$

Water availability affects the single-leaf photosynthetic rate, and the regulation is applicable to canopy scale GPP; the more water is available, the more carbon is assimilated as dry matter (Fig. 4).

4.3.2. Autotrophic respiration: While ARM is independent of water availability, the growth-related component ARC increases with increasing GPP and, thus, with increasing water availability (Fig. 4).

4.3.3. Decomposition: HR (Fig. 4 inset) increases with increasing the volumetric soil water content (SMC_{10} and SMC_{200}) (Witkamp 1966, Meentemeyer 1984):

$$SHR(SMC) = SHR_{SAT} \cdot \frac{SMC}{KM_{SMC} + SMC} \quad (14)$$

where SHR is the specific decomposition rate (Mg C Mg^{-1} C d^{-1}), SHR_{SAT} is the SHR value under water saturation, and KM_{SMC} is the half-saturation coefficient of SMC (fraction). We expect that the model not accounting for the inhibition of decomposition under anaerobic conditions may be applicable to the monthly-step simulation.

4.3.4. NPP and NEP: As shown by Lieth (1975) on the ecosystem level, the annual precipitation-NPP relationship may be well described by a saturation curve

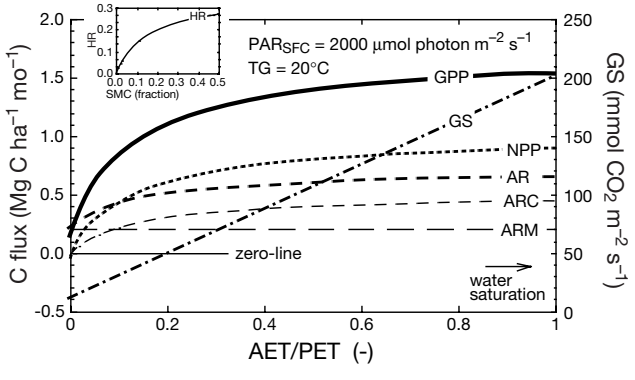

Fig. 4. Environmental responses of ecosystem carbon fluxes to water conditions represented by AET/PET ratio (inset, HR in relation to soil moisture content, SMC). For the water conditions, NEP is not shown, because NPP and HR depend on different water availability indices, and instead water dependence of leaf stomatal conductance (GS) is added

from desert to rain forest. At the physiological level, the water-CD_{ICL} and CD_{ICL}-PC relationships formulated as hyperbolic functions (Eqs. 11 & 12) imply that the water-NPP relationship is well described by a saturation curve (Fig. 4). However, an enhanced GPP leads to higher ARC, and offsets a part of the NPP increase, while ARM is independent of water conditions. Here, we should also take into account the temperature-water interaction, that is, a warmer temperature usually results in greater PET, but not usually in greater AET. Under certain conditions, even if temperature is below the optimum for production, a warmer temperature may aggravate water stress (i.e. smaller AET/PET ratio, GS, and CD_{ICL}) and decrease GPP and NPP.

In consequence, both the water-NPP and water-HR relationships show a hyperbolic-type dependence, and then the water-NEP relationship is not intuitive, because it is the net balance of NPP and HR offsetting each other. Although precipitation is one of the most changeable factors at the seasonal and interannual scales, causing local droughts and floods, a large water pool in groundwater and plant biomass often ameliorates the perturbation of water availability. On the other hand, an anomalously excess precipitation will persist in SWC for the next few months (Manabe & Wetherald 1987). The history effect is a characteristic of the water conditions, making it difficult to estimate the impact of its fluctuation on carbon budget.

4.4. Growth process. In Sim-CYCLE, plant growth rate is strongly controlled by environmental conditions, while partitioning ratio of photosynthate among the plant compartments is assumed to be independent of environment. The dry-matter production theory (Monsi 1960) proposed a plant growth scheme from photosynthesis to reproduction: (1) dead biomass by senescence and herbivory is abandoned from plant body to soil litter, (2) ARM is initially extracted from GPP, (3) the residual photosynthate is partitioned in given ratios among compartments, reflecting the morphological features of plant life forms, and (4) ARC is extracted from each compartment, unless ARM is larger than GPP. A variation of partitioning ratio with proceeding plant growth stage was not necessary for the present purpose, because we were investigating the ecosystem carbon budget after a climax stage was reached.

The seasonality of litterfall characterizes the phenological cycle of biomes, except for evergreen forests (biomes 1, 3, 5, and 6), which have no seasonal change in leaf mortality. The growing period of evergreen forests is determined by the GPP responses to PAR and TG (see Figs. 2 & 3). In deciduous forests, the phenological cycle is prescribed from budbreak to leaf shedding: rainy months in tropical seasonal forests (biome 2), and warm months in temperate deciduous forests (biome 4), e.g. April to October in the northern hemisphere. In the leaf-shedding month, all leaves are abandoned, and in the budbreak month, new foliage system is constructed at the cost of carbon in the stem and root compartments (reallocation). The phenological cycle of grasslands (biomes 7 and 8) is similar to that of deciduous forests, but using mostly root carbon storage in the shoot emergence month. The phenological cycle of croplands is also prescribed, e.g. from cropping in April to harvesting in October in the northern hemisphere. Accompanied with the crop harvest, a part of the aboveground and all of the underground plant biomass is supplied to the litter compartment as detritus.

5. RESULTS

The equilibrium carbon budget is described in Section 5.1, and then interannual change during the 28 yr, accounting for the sensitivity to Q_{10} values, is illustrated in Section 5.2. In Sections 5.3 and 5.4, carbon budget anomalies are statistically related to climatic anomalies through the 28 yr. To facilitate discussion, the grid-based estimations are conveniently grouped into 5 latitudinal zones and 12 biome types. Finally, typical features of the carbon anomaly are exemplified in Section 5.5.

5.1. Average global carbon budget

After reaching an equilibrium through the preliminary iterative calculation, global annual GPP, AR, NPP, and HR were estimated to be 123.5, 60.5, 63.0, and 58.3 Pg C yr^{-1}, respectively. The crop harvest of 3.3 Pg C yr^{-1} and net sequestration of 1.4 Pg C yr^{-1} accounted for the equilibrium state of carbon budget. The estimation of NPP is adequately comparable with those of other models; Cramer et al. (1997) showed that 16 other models estimated NPP to be between 40 and 70 Pg C yr^{-1}. As shown in Fig. 5A, the seasonal change and latitudinal distribution of NPP are also properly retrieved. The global monthly NPP oscillated from 3.3 Pg C mo^{-1} in April to 7.7 Pg C mo^{-1} in July, the seasonality being mainly due to northern high latitudes. Global monthly NEP (figure not shown) was positive, i.e. uptaking carbon, during the northern growing period (1.7 to 2.2 Pg C mo^{-1}), as reflected in the seasonal cycle of the atmospheric CO_2 concentration (e.g. Kohlmaier et al. 1987). Carbon pools in vegetation and soil organic matter were estimated as 545.2 and 1549.6 Pg C, respectively (Fig. 5B). From Table 3, we can see that the variation of carbon budget among the biomes is consistent with observations (e.g. Whittaker

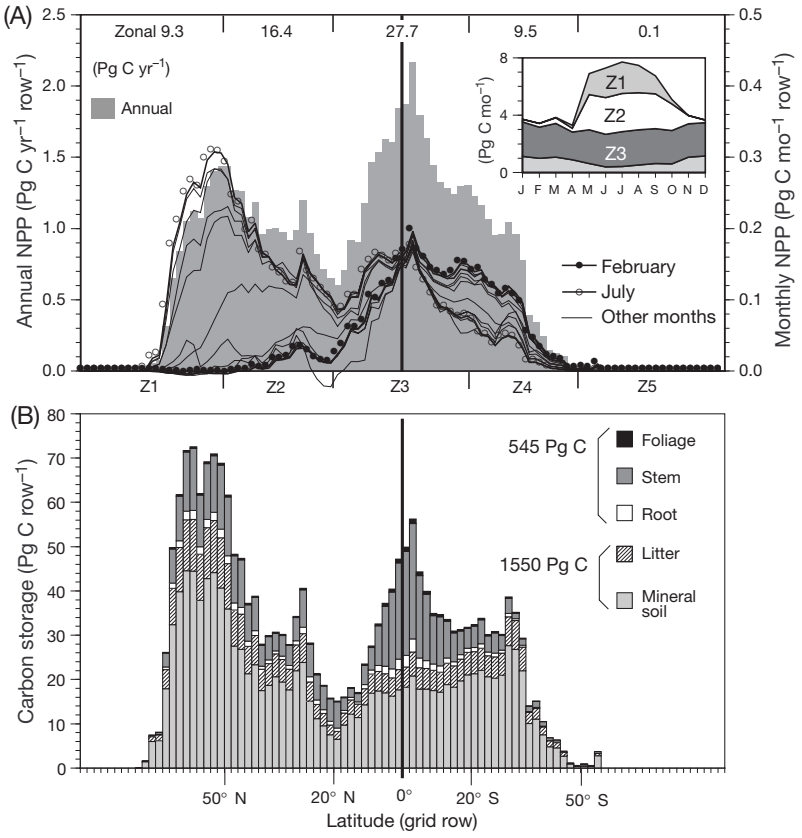

Fig. 5. Latitudinal distributions of estimated productivity and carbon storage at the equilibrium state, for each of 94 grid rows at the T62 resolution. (A) Annual and monthly NPP, in which seasonal change is emphasized by comparing values of July and February. Inset: monthly zonal NPP. (B) Carbon storage in each of the 5 compartments

1975), from tropical rain forest (biome 1), which is productive (NPP: 11.0 Mg C ha^{-1} yr^{-1}) and in which carbon is abundant (C storage: 321.4 Mg C ha^{-1}), to desert (biome 11) which is the most infertile (NPP: 0.2 Mg C ha^{-1} yr^{-1}) and in which carbon is scarce (C storage: 3.7 Mg C ha^{-1}).

5.2. Time-series of global carbon anomalies

In the NCEP/NCAR-reanalysis dataset from 1970 to 1997 (Fig. 6), there were warmer periods such as 1990-1991 and cooler periods such as 1975-1976, and periods with high or low precipitation. The ENSO events and volcanic eruptions, both of which could cause climatic perturbations, are also shown in Fig. 6, but we could not relate the global climate anomalies with these occurrences. In particular regions, however, they exerted notable effects on climate conditions and terrestrial carbon budget (see Section 5.5).

Fig. 7 shows the time-series of monthly carbon flux anomalies. Fig. 8 shows the time-series of monthly ΔNEP, in comparison with the estimation by Keeling et al. (1995) (see Section 6). We can see from them that considerable positive ΔNEPs occurred in 1971 and 1992, and a negative ΔNEP occurred in 1983. Interestingly, the continuous anomalies in ΔAR and ΔHR for several consecutive months led to large cumulative ΔNEPs. For example, the cumulative positive ΔNEP from October 1970 to April 1972 amounts to

Table 3. Average (with standard deviation) climatic conditions and estimated carbon budget for each biome. TG: annual mean surface temperature (°C); PR: annual precipitation (mm yr^{-1}); SWR: annual mean short-wave radiation (W m^{-2}); NPP: estimated annual net primary production (Mg C ha^{-1} yr^{-1}); and C mass: ecosystem carbon storage (Mg C ha^{-1}). The latitudinal zone in which each biome is mainly distributed is given in parenthesis

Biome	Climatic conditions						NPP	SD	C mass	SD
	TG	SD	PR	SD	SWR	SD				
1 (Z3)	23.1	2.6	2489	1032	223	19	11.0	1.1	321	85
2 (Z2)	20.7	5.6	1683	757	240	18	7.7	1.0	235	66
3 (Z2)	14.1	3.4	1443	695	211	19	8.0	2.5	328	116
4 (Z1)	6.3	9.4	821	375	170	26	6.5	2.9	314	158
5 (Z1)	−0.2	3.8	721	250	199	34	5.5	1.7	346	99
6 (Z1)	4.1	15.1	782	580	195	54	3.3	4.2	102	143
7 (Z3)	22.4	2.5	1006	506	263	15	6.0	1.9	134	56
8 (Z3)	14.9	10.4	721	677	246	35	4.4	3.4	104	86
9 (Z2)	15.2	8.7	300	415	252	36	3.8	3.8	144	152
10 (Z1)	−9.9	4.8	365	212	146	12	1.2	2.1	147	228
11 (Z2)	18.8	11.2	71	125	287	30	0.2	0.6	4	13
12 (Z5)	−34.6	13.0	147	240	158	10	0.0	0.0	0	0
Cultivated	14.3	8.0	904	614	229	32	4.9	1.1	74	35

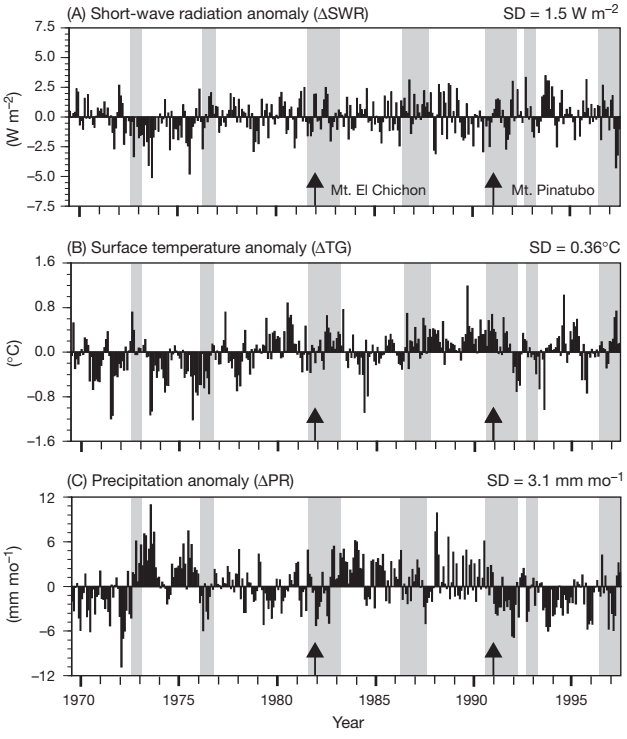

Fig. 6. Anomalies in the global average monthly climate components at the ground surface: (A) irradiance of short-wave radiation (ΔSWR), (B) surface temperature (ΔTG), and (C) precipitation (ΔPR), based on the NCEP/NCAR-reanalysis dataset. Each anomaly is defined as the difference from the 28 yr average. Shaded zones show when ENSO events occurred; arrows indicate extremely large volcanic eruptions, i.e. Mt. El Chichon in 1982 and Mt. Pinatubo in 1991

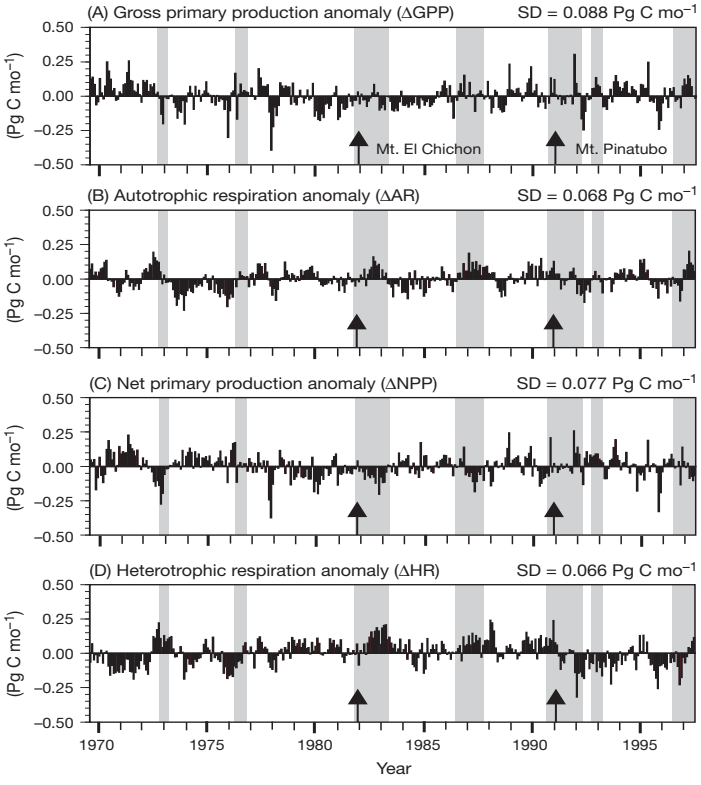

Fig. 7. Anomalies in estimated monthly carbon fluxes: (A) gross primary production (ΔGPP), (B) plant autotrophic respiration (ΔAR), (C) net primary production (ΔNPP), and (D) soil heterotrophic respiration (ΔHR). Shaded zones and arrows show ENSO events and extremely large volcanic eruptions, respectively. Q_{10} value of 2.0 was adopted for ΔAR and ΔHR

+3.80 Pg C, and the negative one from September 1982 to March 1984 amounts to –2.66 Pg C. The estimated time-series of annual NEP deviations using the actual and the average climates are shown in Fig. 9A,B (see Eqs. 2a,b), as well as the net anomaly ΔNEP in Fig. 9C. In addition to Fig. 9C using the standard Q_{10} value of 2.0 for ARM and HR, anomalies using different Q_{10} values, i.e. 1.5 and 2.5, are shown in Fig. 10, because we are aware of their importance for respiration in evaluating the carbon budget anomaly. With a Q_{10} of 2.0, the global ΔNEP fluctuated from –2.06 Pg C yr^{-1} in 1983 to +2.25 Pg C yr^{-1} in 1971 (SD = 1.05 Pg C yr^{-1}), enough to have caused the observed atmospheric CO_2 anomalies. It was found, however, that a larger Q_{10} led to larger ΔNEPs, as represented by the magnitude of standard deviation (from 0.84 Pg C yr^{-1} of Q_{10} = 1.5 to 1.15 Pg C yr^{-1} of Q_{10} = 2.5). Moreover, in some years, the different Q_{10} values led to opposite anomaly tendencies: e.g. in 1974, a positive ΔNEP was estimated by Q_{10} of 2.0 and 2.5 (Figs. 9C & 10B), but a negative one by Q_{10} of 1.5 (Fig. 10A). Another interesting aspect in Fig. 9 is that the 28 yr average ΔNEP was estimated as a positive value (Fig. 9A, +1.35 Pg C yr^{-1}), implying a net carbon sequestration into the biosphere. This enhancement was obviously due to the CO_2 fertilization effect induced by the atmospheric CO_2 rise from 325.5 ppmv in 1970 to 364.5 ppmv in 1997.

Table 4 summarizes the specific contributions to the global ΔNEP trend by each of the carbon fluxes and values of ΔNEP for each of the 4 latitudinal zones (see Table 1, Fig. 5). Apparently, in the years when the biosphere had large ΔNEP (1) both plant and soil, i.e. ΔNPP and ΔHR, acted as net carbon sources and (2) all zones performed similarly either as sinks (e.g. 1971 and 1992) or as sources (e.g. 1973, 1983, and 1988). However, quantitatively and often qualitatively, zonal ΔNEP occurred heterogeneously rather than homogeneously across the biosphere. We can see from Table 4 that the zone with the most influence on the global ΔNEP trend was Z3 (i.e. tropics), which is mainly occupied by such ecologically and biogeochemically active biomes as tropical rain forest (biome 1) and which is responsible for nearly half (27.7 Pg C yr^{-1}) of the global annual NPP. Z3 affects global ΔNEP

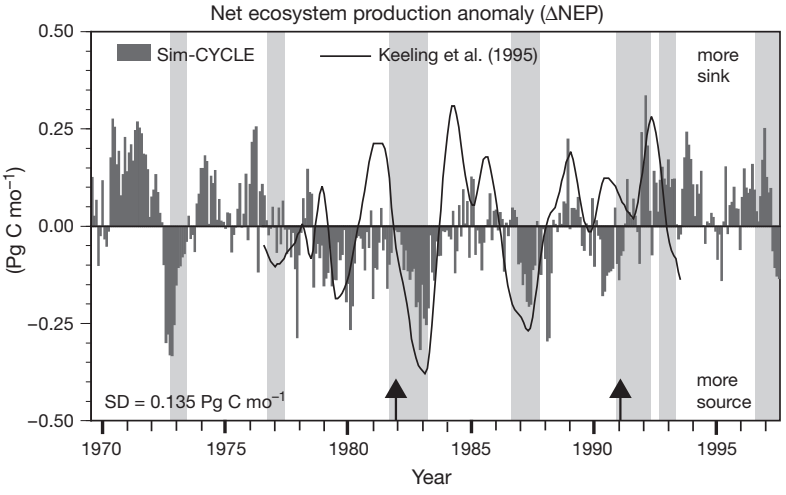

Fig. 8. Anomalies in estimated monthly net ecosystem production (ΔNEP) derived from Fig. 7. The result of Keeling et al. (1995), derived from the atmospheric CO_2 data, is illustrated with a line, for a comparison. Shaded zones and arrows show ENSO events and extremely large volcanic eruptions, respectively

critically in both directions (either sink or source), except for only 4 (i.e. 1970, 1981, 1992, and 1995) of the 28 years. However, in 3 (1970, 1981, and 1995) out of these 4 years, the biosphere was nearly neutral with respect to the carbon balance (i.e. ΔNEP < SD). The standard deviations of zonal ΔNEPs also suggest the outstanding contribution by the tropical zone Z3, such that it had by far the largest SD (±0.66 Pg C yr^{-1}) among the 4 zones, accounting for over half of the global total.

5.3. Multiple regression analysis

Statistical analyses were conducted so as to derive some relationships between climatic anomalies (Fig. 6) and carbon flux anomalies (Table 4, Figs. 7 & 8). At first, we conducted a multiple regression analysis for the 3 independent climatic variables, ΔTG, ΔPR and ΔSWR. Since the term ΔTG had high correlations with ΔTS_{10} and ΔTS_{200} ($p < 0.001$), we applied it also to ΔHR. Although PR itself was not used as an input to the simulation experiment, we regarded it as a plain indicator of water availability, rather than Δ(AET/PET), which would be contaminated by ΔTG.

Table 5 shows the standardized correlation coefficients calculated for the global biosphere and the 4 latitudinal zones (Z1 to Z4). In Table 5A, the raw coefficient values are also listed for the global analysis, which shows the responsiveness of the biospheric carbon flux to climate anomalies. Apparently, ΔAR and ΔHR had significant positive correlations with ΔTG in all regions; this leads to a high negative correlation of ΔNEP with ΔTG, globally and zonally, even during the growing period. The highest negative correlation between ΔTG and ΔNEP (standardized correlation coefficient = −0.919, $p < 0.001$) emerged in Z3, which is almost completely occupied by tropical evergreen forests (biome 1) and grasslands (biome 8). In these warm biomes, respiration (both AR and HR) had the highest sensitivity to temperature, as expected from the exponential dependence of both types of respiration (see Eqs. 9 & 10, Fig. 3). On the other hand, ΔGPP and ΔNPP were less sensitive to climatic anomalies. In Z1 and Z3 (Table 5C,E), ΔPR and ΔSWR had a weak influence on

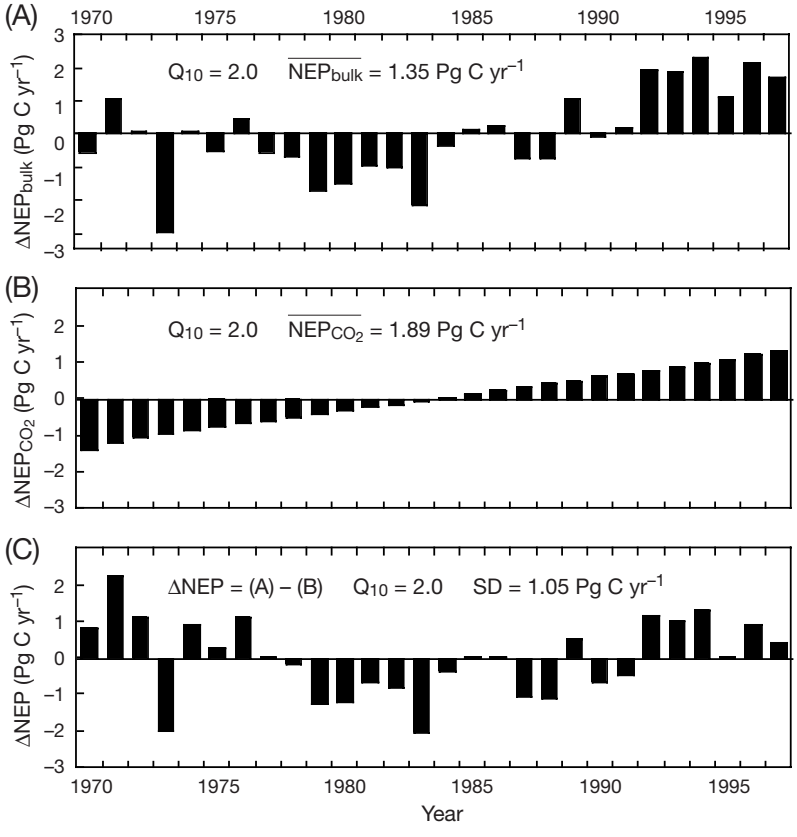

Fig. 9. Annual anomalies in estimated net ecosystem production (ΔNEP): (A) deviation using the actual climate data (see Eq. 2), (B) deviation using the average climate data, representing the CO_2 fertilization effect on the carbon budget, and (C) net anomaly ΔNEP induced by the climatic variability. The standard Q_{10} value of 2.0 was adopted for AR and HR

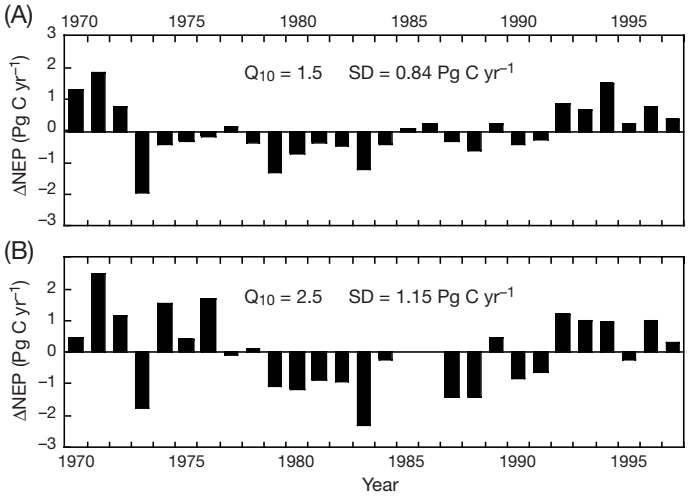

Fig. 10. Annual anomalies in estimated net ecosystem production (ΔNEP) derived similarly to Fig. 9C, but assuming different temperature sensitivity for AR and HR: (A) Q_{10} = 1.5 and (B) Q_{10} = 2.5

ΔGPP and ΔNPP, while ΔTG had a moderate effect. In Z2, which contains broad areas of arid ecosystems (biomes 8, 9, and 11), higher precipitation resulted in accelerated soil decomposition (ΔHR), but little change in primary productivity (both ΔGPP and ΔNPP): thus, ΔPR and ΔNEP were negatively correlated (Table 5D). The sensitivity of ΔGPP and ΔNPP to ΔTG varied among the latitudinal zones, which differ in habitat temperature conditions and dominant biome type correspondingly. For example, ΔGPP and ΔNPP in the cooler zone Z1 had positive correlations with ΔTG (Table 5C), while those in the warmer zones Z3 and Z4 had negative ones (Table 5E,F).

5.4. Linear regression analysis

Next, we conducted a linear regression analysis to simplify and quantify the relationship between ΔTG (the most overriding factor, as shown in Table 5) and carbon flux anomalies, that is, $\Delta F = \beta \cdot \Delta TG$ (β is the slope).

5.4.1. Annual basis

As shown in Fig. 11, the ΔGPP had little correlation with ΔTG (r^2 = 0.01, p = 0.58), while the ΔAR and ΔHR had stronger correlations (r^2 = 0.46, p < 0.001 and r^2 = 0.33, p = 0.0015, respectively) and steeper slopes β_{ann} = +1.46 and +1.57 Pg C yr^{-1} °C^{-1}, respectively). The ΔNPP which is the balance of ΔGPP and ΔAR, had a moderate negative correlation with ΔTG (β_{ann} = –1.21 Pg C yr^{-1} °C^{-1}, r^2 = 0.33, p = 0.0015). Since ΔNEP is the balance of ΔGPP, ΔAR, and ΔHR, it had a considerable negative correlation (r^2 = 0.38, p < 0.001). The highest negative β_{ann} (–2.69 Pg C yr^{-1} °C^{-1}) between ΔTG and ΔNEP suggests that a significant amount of carbon would be immediately released from the biosphere to the atmosphere as a result of a small global warming; precipitation anomalies may make deviations from the regression line (Fig. 11E).

5.4.2. Monthly basis

A monthly-based analysis was also conducted: slope β_{mon} (Pg C mo^{-1} °C^{-1}) (Fig. 12). ΔGPP shows a biannual

Table 4. Estimated annual global carbon flux anomalies, for the case of Q_{10} = 2.0. Zonal values are also listed for ΔNEP (Z5 was negligible). Exemplified years in text, i.e. 1971, 1983, and 1992, are shaded. The maximum and minimum in each column are given in **bold**

Year	Annual carbon flux anomaly (Pg C yr^{-1})								
	ΔGPP	ΔAR	ΔNPP	ΔHR	ΔNEP				
					Global	Z1	Z2	Z3	Z4
1970	**1.00**	0.74	0.26	–0.55	0.82	0.02	0.23	0.21	**0.35**
1971	0.92	–0.34	**1.25**	**–1.06**	**2.25**	0.15	**0.51**	**1.32**	0.27
1972	0.72	0.42	0.30	–0.82	1.10	–0.02	0.32	0.61	0.18
1973	–0.46	0.23	–0.69	**1.34**	–2.00	–0.19	–0.29	–1.04	**–0.48**
1974	–0.56	**–1.22**	0.66	–0.27	0.90	–0.19	0.37	0.87	–0.13
1975	0.05	–0.43	0.48	0.21	0.26	–0.19	–0.06	0.36	0.14
1976	–0.41	–0.90	0.48	–0.71	1.13	–0.16	0.37	0.67	0.26
1977	0.57	0.40	0.17	0.13	0.03	0.01	–0.11	0.23	–0.10
1978	–0.57	–0.19	–0.38	–0.18	–0.18	–0.11	–0.05	–0.07	0.05
1979	0.11	0.45	–0.34	0.90	–1.28	–0.09	0.01	–1.06	–0.13
1980	**–0.89**	0.17	**–1.06**	0.21	–1.19	–0.15	–0.14	–0.75	–0.14
1981	–0.68	–0.34	–0.35	0.36	–0.68	**–0.30**	–0.21	–0.27	0.10
1982	–0.34	0.04	–0.39	0.43	–0.83	–0.01	–0.24	–0.62	0.04
1983	–0.34	0.52	–0.86	1.25	**–2.06**	–0.27	**–0.36**	**–1.19**	–0.24
1984	–0.72	–0.74	0.02	0.39	–0.37	0.03	0.01	–0.23	–0.18
1985	–0.50	–0.40	–0.10	–0.11	0.03	0.08	–0.17	0.25	–0.13
1986	0.10	–0.10	0.20	0.15	0.05	0.04	–0.14	0.30	–0.15
1987	0.31	**0.82**	–0.50	0.59	–1.05	0.06	–0.25	–0.78	–0.08
1988	–0.19	0.27	–0.46	0.69	–1.11	–0.18	–0.30	–0.62	–0.01
1989	0.19	–0.40	0.58	–0.00	0.55	0.03	0.04	0.43	0.05
1990	0.45	0.61	–0.16	0.54	–0.68	0.18	–0.25	–0.53	–0.08
1991	–0.00	0.23	–0.23	0.32	–0.48	0.19	–0.26	–0.43	0.02
1992	–0.11	–0.46	0.35	–0.82	1.14	**0.28**	0.41	0.37	0.09
1993	0.11	–0.18	0.29	–0.69	0.99	0.16	0.29	0.48	0.06
1994	0.76	0.20	0.55	–0.76	1.30	0.28	–0.09	0.82	0.29
1995	0.53	0.57	–0.04	–0.06	0.01	0.15	0.03	–0.33	0.16
1996	–0.52	–0.44	–0.08	–1.03	0.93	0.07	0.24	0.45	0.17
1997	0.46	0.44	0.02	–0.44	0.42	0.15	0.09	0.55	–0.38
SD	0.53	0.52	0.51	0.66	1.05	0.16	0.25	0.66	0.20

Table 5. Standard correlation coefficients between the anomalies in carbon fluxes and the anomalies in climatic factors: surface temperature (ΔTG), precipitation (ΔPR), and irradiance (ΔSWR). To offset the scale difference among the climatic factors, standardized correlation coefficients are listed (**p < 0.001; *p < 0.01), except for (A), which lists the raw correlation coefficients. Note that TG and SWR are model input data, but PR is not

	ΔTG (°C)	ΔPR (mm)	ΔSWR (W m^{-2})	r^2
(A) Global/raw (Pg C yr^{-1})				
ΔGPP	0.359	−0.013	−0.066	
ΔAR	1.553	−0.009	−0.079	
ΔNPP	−1.194	−0.004	0.013	
ΔHR	1.529	0.018	−0.119	
ΔNEP	−2.646	−0.022	0.146	
(B) Global/standardized				
ΔGPP	0.161	−0.516	−0.075	0.146
ΔAR	0.721**	−0.355	−0.093	0.500
ΔNPP	−0.564*	−0.181	0.016	0.284
ΔHR	0.557**	0.576**	−0.110	0.702
ΔNEP	−0.602**	−0.435*	0.085	0.561
(C) Z1 (N. high)/standardized				
ΔGPP	0.654**	−0.368	−0.245	0.541
ΔAR	0.715**	−0.408	−0.142	0.613
ΔNPP	0.594*	−0.329	−0.306	0.473
ΔHR	0.689**	0.320	−0.089	0.667
ΔNEP	−0.055	−0.755*	−0.277	0.282
(D) Z2 (N. middle)/standardized				
ΔGPP	0.476	−0.188	−0.495	0.212
ΔAR	0.843**	−0.100	−0.085	0.630
ΔNPP	−0.172	−0.143	−0.548	0.262
ΔHR	0.538**	0.526**	0.186	0.577
ΔEP	−0.475*	−0.481*	−0.402	0.560
(E) Z3 (Tropical)/standardized				
ΔGPP	−0.367	−0.399	0.311	0.416
ΔAR	0.684**	−0.360	0.012	0.626
ΔNPP	−0.993**	−0.021	0.274*	0.923
ΔHR	0.717**	0.291	−0.359	0.667
ΔNEP	−0.919**	−0.160	0.336*	0.858
(F) Z4 (S. middle)/standardized				
ΔGPP	−0.377	−0.476	−0.136	0.142
ΔAR	0.437	−0.252	0.067	0.232
ΔNPP	−0.871**	−0.371	−0.233	0.699
ΔHR	0.338*	0.580*	−0.276	0.683
ΔNEP	−0.716**	−0.593*	0.054	0.771

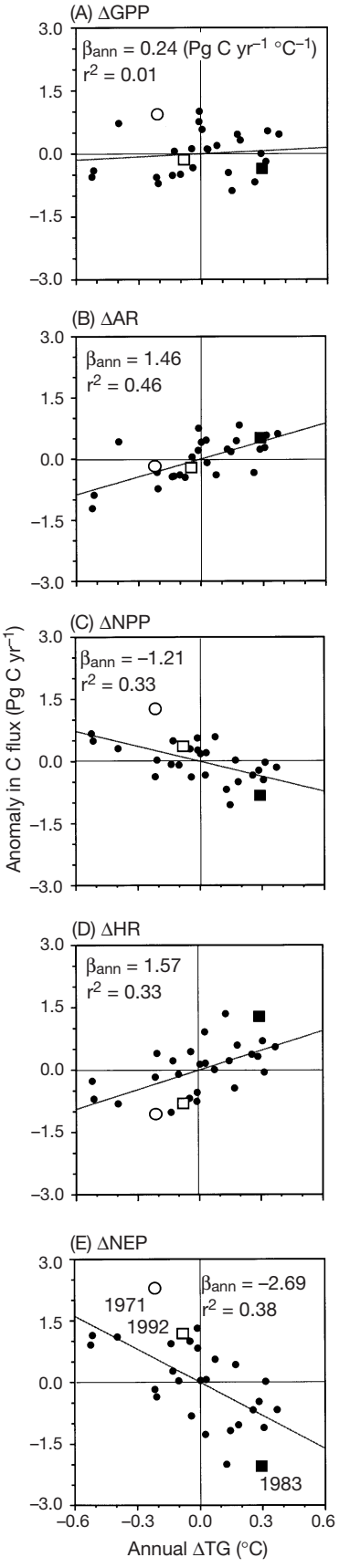

Fig. 11. Correlations between anomalies in annual mean global surface temperature (ΔTG) and anomalies in estimated annual total carbon fluxes (n = 28, from 1970 to 1997) (for the case of Q_{10} = 2.0): (A) ΔGPP, (B) ΔAR, (C) ΔNPP, (D) ΔHR, and (E) ΔNEP. The slope (β_{ann}) and correlation coefficient (r^2) of each regression line are given in each panel. The exemplified years in the text are shown: (○) 1971, (■) 1983, and (□) 1992

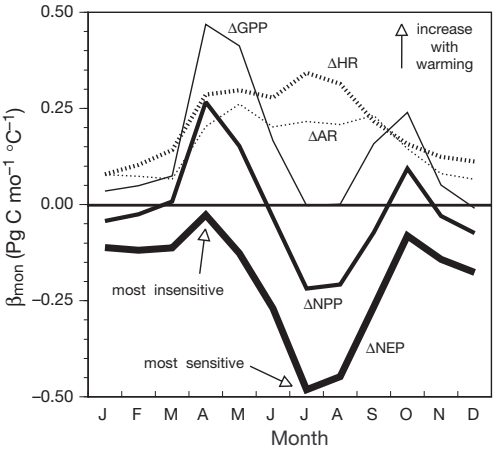

Fig. 12. Seasonal changes in the sensitivity of the estimated monthly global carbon flux anomalies (Q_{10} = 2.0) to the monthly air temperature anomalies, as represented by the slope of linear regressions (β_{mon})

oscillation with 2 peaks; one shows a strong positive dependence on ΔTG in April and May (spring in the northern hemisphere), and the other occurs, to a lesser extent, in September and October (autumn), whereas there is virtually no dependence in July and August (mid-summer in the northern hemisphere) and in November to March (winter). Apparently, the substantial dependencies in spring and autumn are due to the multiple temperature effect on physiological activities (see Eq. 7) and on phenological stimulation (i.e. elongation of growing period). In summer, in contrast, because most ecosystems are largely under their thermal optima, their ΔGPPs are susceptible to neither physiological nor phenological effects of the temperature fluctuation. ΔAR had a positive slope irrespective of season; therefore, β_{mon} of ΔNPP varied almost in parallel with that of ΔGPP, i.e. positive in spring and in autumn in the northern hemisphere, and negative in summer and in winter in the northern hemisphere. Similarly, HR had a consistently positive β_{mon} throughout the year. Finally, ΔNEP had a strong negative slope exceeding –0.4 Pg C mo^{-1} °C^{-1} from June to August (Fig. 12).

We analyzed the spatial heterogeneity as well as monthly change in the relationship between ΔTG and ΔNEP. As shown in Fig. 13, tropical ecosystems in Z3 had negative correlations with ΔTG irrespective of seasons, whereas temperate ecosystems in Z2 and boreal ones in Z1 showed a clear seasonal change. In summer and winter, most of them had negative correlations ($r < 0$), while in spring and autumn, these ecosystems had significantly positive ones ($r > 0$), because a warmer temperature leads to a longer growing period. As a result, global ΔNEP had a weaker correlation with ΔTG in spring and autumn months (e.g. r = –0.068 in April), although locally some ecosystems had substantial responsiveness. These seasonal changes deserve our attention when considering the impacts of climate change on the biospheric carbon budget.

5.5. Examples of three extreme ΔNEP years

To elucidate the underlying mechanism of large ΔNEPs, we examine features in 3 interesting years: the largest negative ΔNEP in 1983 (–2.06 Pg C yr^{-1}), the largest positive ΔNEP in 1971 (+2.25 Pg C yr^{-1}), and the accidental positive ΔNEP in 1992 (a sink year, +1.14 Pg C yr^{-1}). These years are identified in Fig. 11 and listed in Table 4.

5.5.1. 1983: a strong ENSO year

5.5.1.1. Global maps. Most of the climatic anomalies in 1983 may be relevant to the robust ENSO event, which began in early 1982. Accompanied by a sea-surface temperature rise in the eastern Pacific Ocean, coastal regions of South America had positive ΔTG (Fig. 14A). The positive ΔTG was also evident in Eurasian regions. From the precipitation anomaly map shown in Fig. 14B, we can find a larger spatial heterogeneity from positive ΔPRs in South America and part of Monsoon Asia to negative ones in Africa. Fig. 14C shows a global distribution of ΔNEP values which were affected by ΔTG and ΔPR in 1983, where many tropical ecosystems and some temperate ecosystems in Europe and North America acted as net carbon sources, while little net carbon sequestration happened in other areas (e.g. a part of South Africa). Especially equatorial South America which had warmer temperatures and high precipitations emitted a large amount of carbon.

5.5.1.2. Zonal distribution of anomalies. Table 4 shows that the carbon emission was especially evident in Z3 (–1.19 Pg C yr^{-1}), which is the most sensitive to ΔTG among the 4 zones. In 1983, Z3 underwent a large positive ΔTG of +0.39°C and a moderate negative ΔPR of –12 mm yr^{-1}. The anomalously high temperature in 1983 was particularly evident from February to July (+0.69°C, see Fig. 6B), and it enhanced respiration and decomposition in the tropical ecosystems. We can see from Table 4, summarizing global and zonal anomalies, that not only Z3 but also Z2 had the largest negative ΔNEP (–0.36 Pg C yr^{-1}); Z1 had the second largest negative (–0.27 Pg C yr^{-1}) and Z4 had the third largest negative ΔNEP (–0.24 Pg C yr^{-1}) during the 28 yr. These simultaneous anomalies strongly suggest the impacts of a climate perturbation at the global scale.

5.5.1.3. Biome-specific aspects. Table 6 summarizes such biome-specific features as climate sensitivity and

Table 6. Biome-specific features in 1983 and 1992: ΔTG, ΔPR, and ΔNEP, for the case of Q_{10} = 2.0. The latitudinal zone in which each biome is mainly distributed is given in parenthesis

Biome	β_{ann} (slope of regression)		1983 (robust ENSO year)				1992 (post-Mt. Pinatubo-eruption year)			
	ΔTG-ΔNEP (Mg C ha^{-1} yr^{-1} °C^{-1})	ΔPR-ΔNEP (Mg C ha^{-1} yr^{-1} 100mm^{-1})	ΔTG[a] (°C)	ΔPR[a] (mm yr^{-1})	ΔNEP (Mg C ha^{-1} yr^{-1})	ΔNEP (Pg C yr^{-1})	ΔTG[a] (°C)	ΔPR[a] (mm yr^{-1})	ΔNEP (Mg C ha^{-1} yr^{-1})	ΔNEP (Pg C yr^{-1})
1 (Z3)	−1.31	−0.10	0.41	9.1	−0.50	−0.61	−0.00	−1.5	0.22	0.27
2 (Z2)	−0.71	−0.15	0.09	77.2	−0.26	−0.17	−0.13	−127.3	0.21	0.14
3 (Z2)	−0.27	−0.13	0.07	73.3	−0.24	−0.03	−0.32	−54.0	0.29	0.04
4 (Z1)	−0.27	−0.19	0.68	59.1	−0.12	−0.14	0.16	−77.3	0.20	0.22
5 (Z1)	0.01	−0.23	0.46	67.2	−0.19	−0.18	0.23	−57.5	0.18	0.17
6 (Z1)	−0.16	−0.06	0.41	−31.6	−0.19	−0.14	−0.12	−1.2	0.06	0.05
7 (Z3)	−0.36	−0.14	0.51	−43.5	−0.04	−0.02	0.31	−16.5	−0.14	−0.06
8 (Z3)	−0.27	−0.16	0.32	12.5	−0.18	−0.49	−0.05	−29.6	0.07	0.20
9 (Z2)	−0.17	−0.15	0.26	33.2	−0.07	−0.09	−0.22	19.0	−0.00	−0.00
10 (Z1)	−0.00	0.02	0.09	−2.5	−0.04	−0.02	−0.44	−16.1	0.03	0.02
11 (Z2)	−0.00	−0.01	−0.15	−1.6	−0.00	−0.002	−0.42	5.3	−0.00	−0.007
Cultivated	−0.18	−0.09	0.26	28.8	−0.10	−0.15	0.01	−48.2	0.07	0.11
Total[b]	−0.27	−0.20	0.30	22.4	−0.16	−2.06	−0.07	−29.1	0.09	1.14

[a]Long-term mean conditions are listed in Table 3; [b]area-weighted average excluding ice sheets (biome 12)

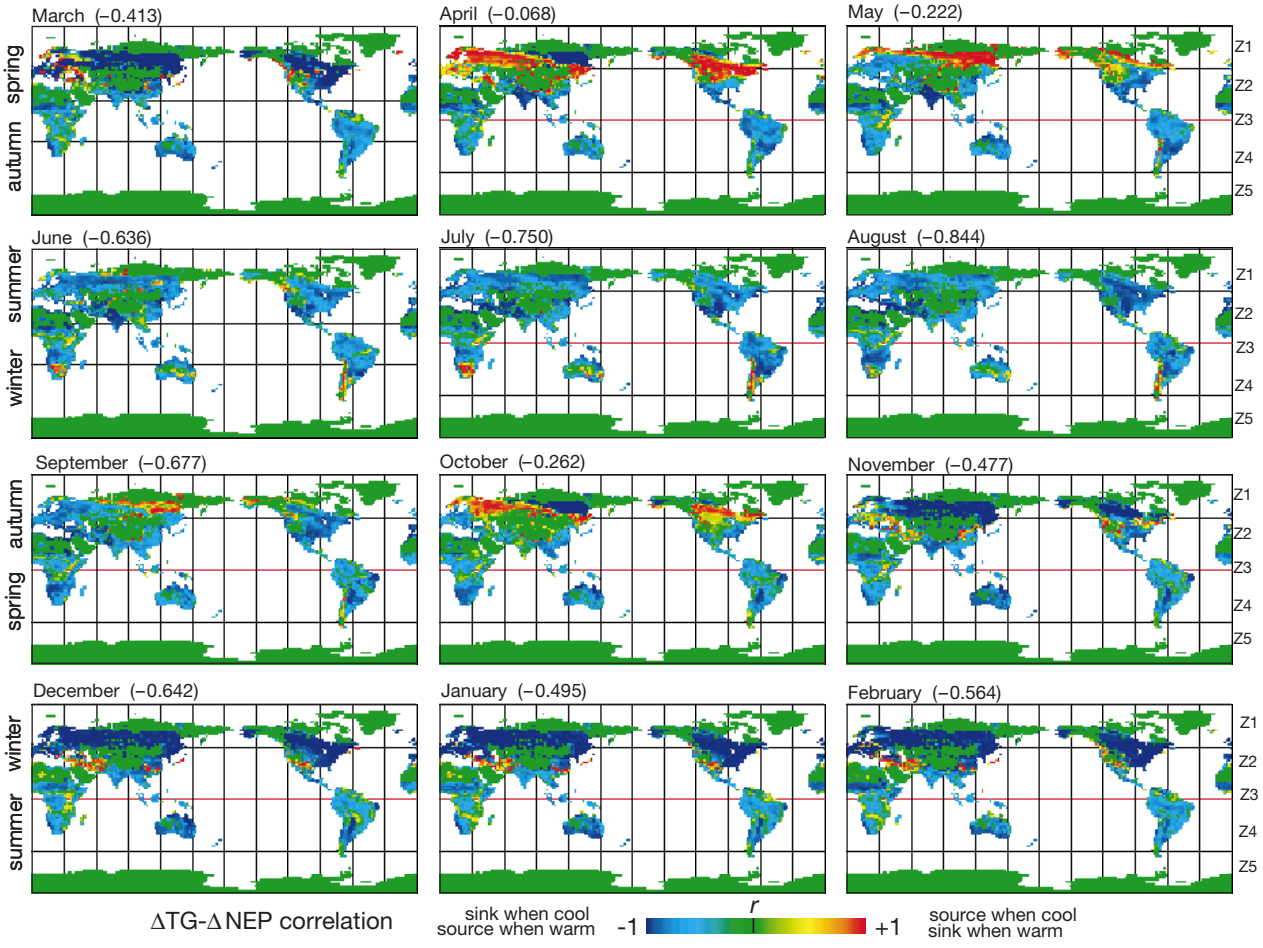

Fig. 13. Global maps of the seasonal change in the correlation coefficient (r) between monthly ΔTG and ΔNEP (Q_{10} = 2.0), from 1970 to 1997. When it has a positive/negative value (in yellow to red/blue), a more active sink or a less active source of carbon is induced by an anomalously warmer/cooler temperature, respectively. The global averages are given in parentheses

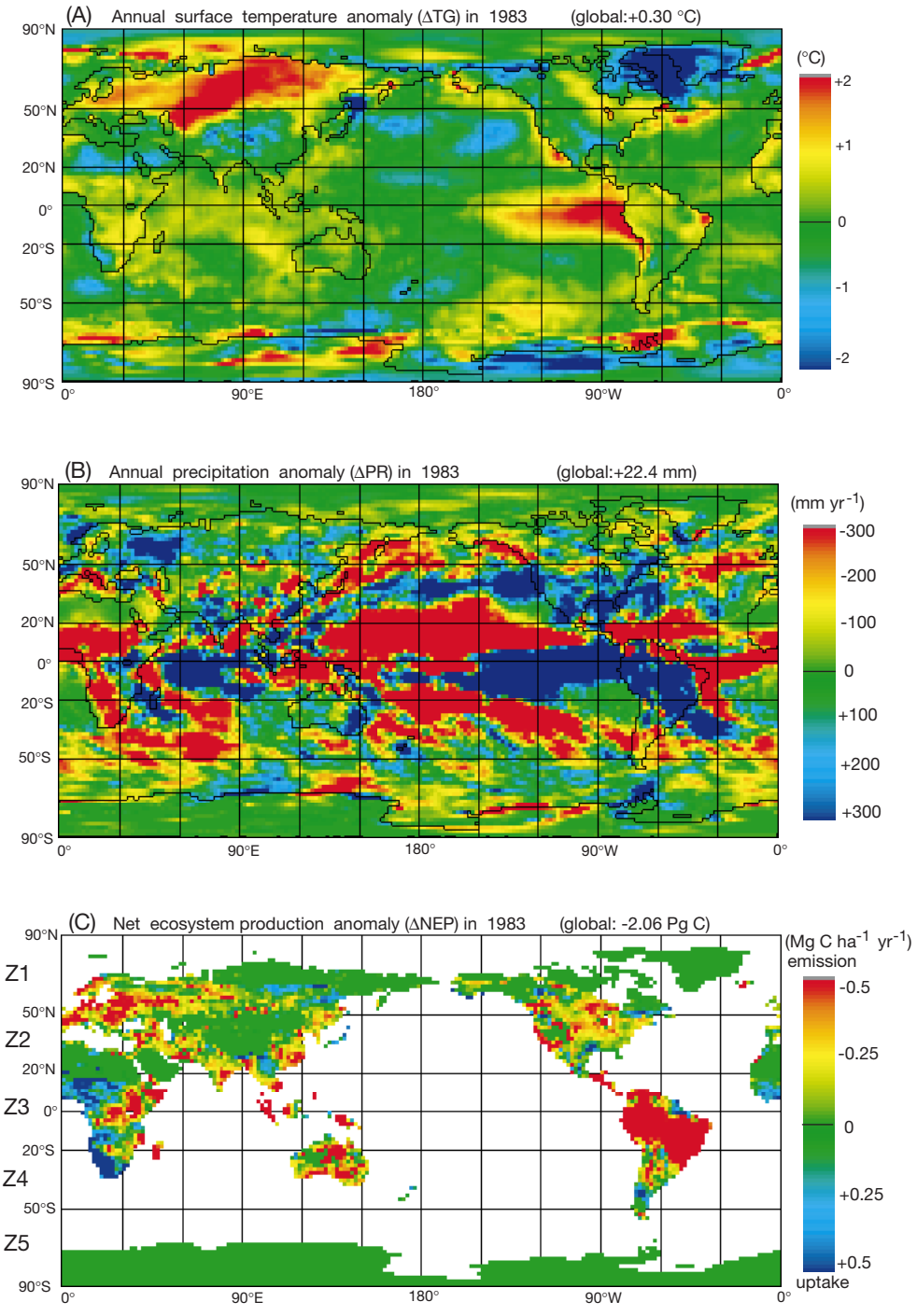

Fig. 14. Global maps of the annual climatic anomalies and resultant net ecosystem carbon balance in 1983, a typical ENSO year. (A) NCEP/NCAR-reanalysis surface temperature ΔTG, (B) NCEP/NCAR-reanalysis precipitation ΔPR, and (C) net ecosystem production ΔNEP estimated by Sim-CYCLE using $Q_{10} = 2.0$

contribution to global ΔNEPs. In 1983, most biomes had significantly negative ΔNEPs, especially in tropical evergreen forests (biome 1, –0.61 Pg C yr^{-1}) and grasslands (biome 8, –0.49 Pg C yr^{-1}). These biomes are the major components in Z3 and are sensitive to ΔTG and ΔPR (see β_{ann} in Table 6); a positive ΔTG (+0.3~0.4°C) in these ecosystems is likely to be the principal cause of the global ΔNEP. This result is consistent with the

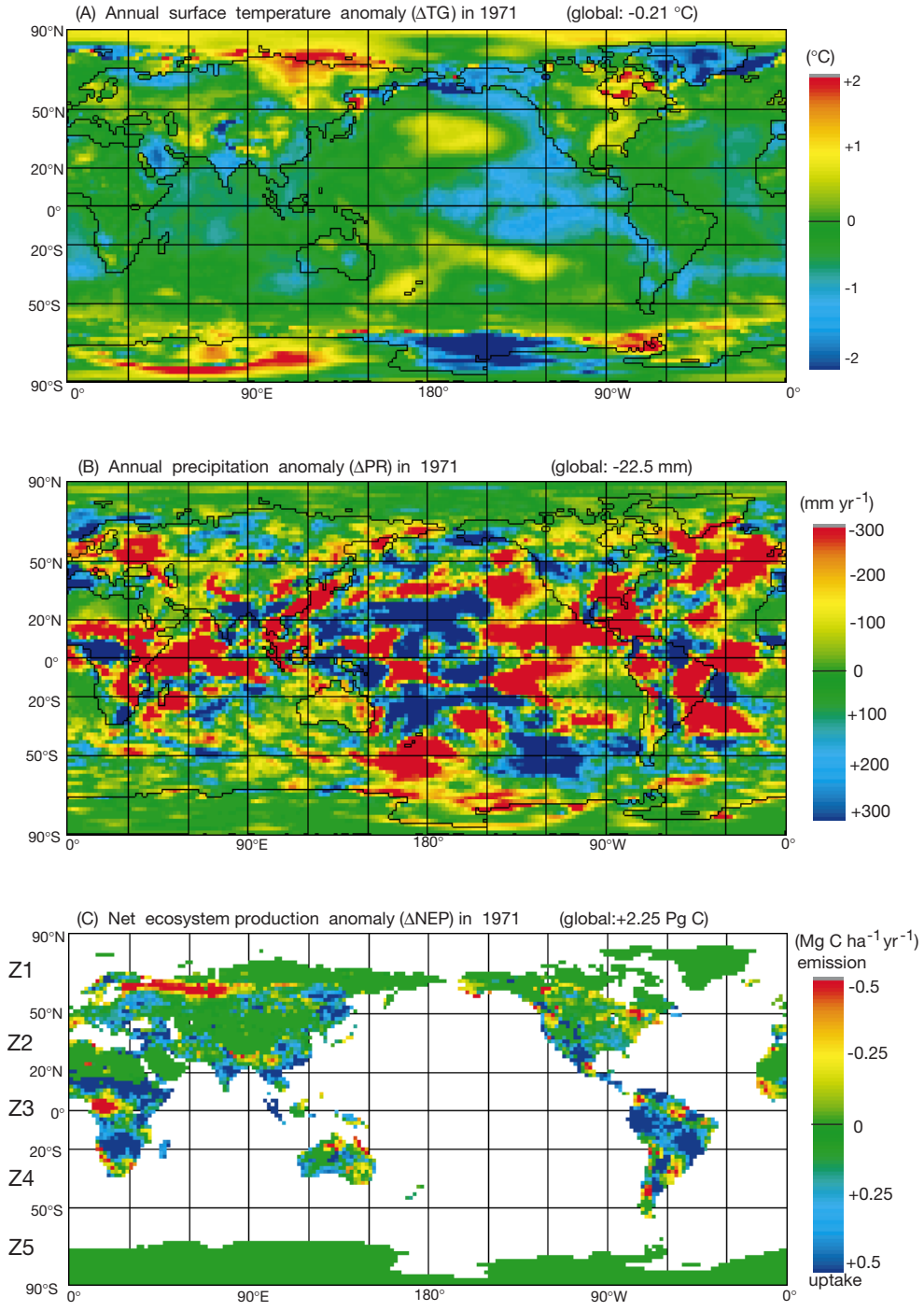

Fig. 15. Global maps of the annual climatic anomalies and resultant net ecosystem carbon balance in 1971, the largest positive ΔNEP year. (A) NCEP/NCAR-reanalysis surface temperature ΔTG, (B) NCEP/NCAR-reanalysis precipitation ΔPR, and (C) net ecosystem production ΔNEP estimated by Sim-CYCLE using $Q_{10} = 2.0$

analysis by Gérard et al. (1999). In contrast, however, savannas (biome 7), which are mainly occupied with C_4 grasses, exerted little effect on the global carbon budget, in spite of a large temperature anomaly (+0.5°C).

5.5.2. 1971: the largest positive ΔNEP year

5.5.2.1. Global maps. The largest positive global ΔNEP took place in 1971 (+2.25 Pg C). This is interesting as a

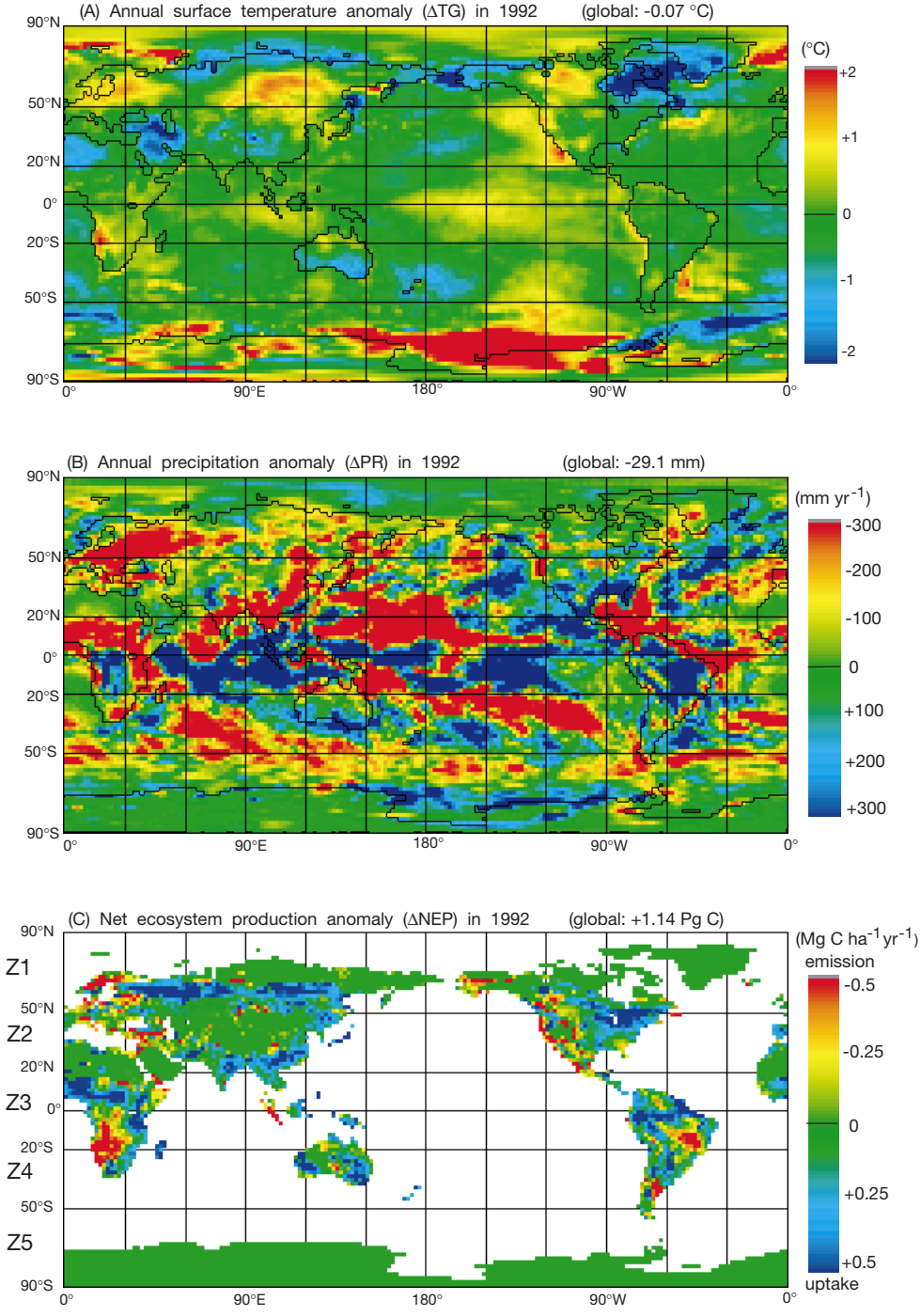

Fig. 16. Global maps of the annual climatic anomalies and resultant net ecosystem carbon balance in 1992, subsequent to the Mt. Pinatubo eruption in June 1991. (A) NCEP/NCAR-reanalysis surface temperature ΔTG, (B) NCEP/NCAR-reanalysis precipitation ΔPR, and (C) net ecosystem production ΔNEP estimated by Sim-CYCLE using $Q_{10} = 2.0$

contrast to the largest negative anomaly in 1983. In 1971, a La Niña year, eastern Pacific sea-surface temperature was lower than average (Fig. 15A), and correspondingly global ground surface was cooler than the average by –0.21°C (see Fig. 6B). Although most tropical regions experienced moderate temperatures, they had considerable negative ΔPR, especially in South America, Africa, and Monsoon Asia (Fig. 15B). Thus, the distribution of carbon anomaly ΔNEP (Fig. 15C) seems likely to be related to the negative ΔPR rather than ΔTG. For example, in Africa, the distribution of ΔNEP was apparently comparable to that of ΔPR.

5.5.2.2. Zonal distribution of anomalies. In 1971, because Z3 underwent a negative ΔTG (–0.34°C) and a negative ΔPR (–47 mm yr^{-1}), it had the largest positive zonal ΔNEP of +1.32 Pg C yr^{-1} (Table 4). Both lower temperature and precipitation reduce carbon emissions by respiration (ΔAR of –0.34 Pg C yr^{-1}) and decomposition (ΔHR of –1.06 Pg C yr^{-1}), as fully explained by the multiple regression analysis in Section 5.3. Also, note that the year 1971 had the largest positive ΔNPP of +1.25 Pg C yr^{-1}, due to both positive ΔGPP and negative ΔAR (Table 4).

5.5.3. 1992: after the Mt. Pinatubo eruption

5.5.3.1. Global maps. Although annual average temperature in 1992 was lower than that in the previous year 1991 by –0.35°C (see Fig. 6B), the temperature anomalies in 1992 (Fig. 16A) seem more gentle than those in 1983. Nevertheless, we can find some cooler (e.g. Middle East and northeastern North America) and warmer (e.g. Siberia and western North America) regions. As shown in Fig. 16C, ΔNEP values in 1992 in many ecosystems were positive, especially those in South America, North America, Monsoon Asia, and Australia. The large carbon sink in Monsoon Asia seems consistent with (maybe ENSO-induced) negative ΔPR (Fig. 16B) which could reduce decomposition (see Table 5).

5.5.3.2. Zonal distribution of anomalies. In 1992, the zone contributing most to ΔNEP was the northern middle zone Z2 (+0.28 Pg C yr^{-1}), which had a negative ΔTG (–0.2°C) and ΔPR (–27.8 mm yr^{-1}), but insignificant ΔPAR_{SFC}. The cooler temperature was especially evident from July to October (–0.79°C in Z1 and –0.49°C in Z2), which was certainly induced by the Mt. Pinatubo eruption in June 1991. As McCormick et al. (1995) summarized, the eruption was so robust that it gave rise to a series of chemical, optical, and climatic ramifications, leading to a global tropospheric cooling in the following few years (see Fig. 6B). Additionally, PAR_{SFC} showed little anomaly (see Fig. 6A) in spite of the eruption, because the attenuation of direct radiation could be compensated by increased diffused solar radiation; the latter contains a larger fraction of PAR than direct radiation (Alados-Arboledas et al. 1997). Consequently, lower temperature and precipitation resulted in reduced rates of respiration (ΔAR = –0.46 Pg C yr^{-1}) and decomposition (ΔHR = –0.82 Pg C yr^{-1}).

5.5.3.3. Biome-specific aspects. In 1992, the biome exerting the largest influence on ΔNEP was still tropical evergreen forests (+0.27 Pg C yr^{-1}). Moreover, temperate deciduous forests (biome 4) and temperate and boreal needle-leaved forests (biome 5) in Z1 also made noteworthy positive contributions (+0.22 and +0.17 Pg C yr^{-1}, respectively). Table 6 lists the annual global ΔTG in which cooling is not so evident, but the northern regions had larger negative ΔTG by about –0.4°C from April to October, which include the sensitive months (see Fig. 11). Low precipitations (–29 mm yr^{-1}) that could reduce soil moisture affected ΔNEP by limiting the rate of decomposition.

6. DISCUSSION

The multiple and linear regression analyses, shown in Figs. 11 to 13 and Table 5, strongly suggest that the biospheric global carbon budget ΔNEP is sensitive to climatic anomalies, primarily in temperature and secondarily in precipitation. Since these outcomes are critically dependent on the characteristics of the simulation model used, we should carefully examine whether the sensitivity is truly due to those of the biosphere or those of Sim-CYCLE, i.e. an artifact. The formulations of carbon dynamics dependent on various environmental factors, such as Eqs. (3) to (14), are simple but would capture a physiological-scale response properly. However, there remain uncertainties about the strength of these sensitivities. Yokota & Hagihara (1996) observed that the Q_{10} value of woody plant respiration changed seasonally (i.e. larger in winter and smaller in summer), and Knorr & Heimann (1995) concluded that the most appropriate value of Q_{10} for biospheric respiration (global ΔAR and ΔHR) was 1.5, rather than 2.0 (observed *in situ* frequently, and adopted by Sim-CYCLE). Our sensitivity analysis also suggests the importance of determining Q_{10} values in appraising the CO_2 budget, and the results using Q_{10} = 1.5 may indicate the lower end of biospheric response, and those using Q_{10} = 2.5 the higher end.

The following facts may allow us to confirm the credence of the model analyses presented in this paper: (1) Sim-CYCLE simulated the features of the contemporary terrestrial carbon budget well and (2) our model analyses agreed satisfactorily with the estimation of ΔNEP derived from analyses of atmospheric CO_2 and its stable carbon isotopic composition (Keeling et al. 1995, Joos et al. 1999). In fact, the simulated monthly ΔNEP trend agrees with one by Keeling et al. (1995) (line in Fig. 8), who estimated the net terrestrial and ocean carbon exchanges based on the anomalies in the atmospheric CO_2 concentration and its stable carbon isotopic composition. For example, in 1983 and 1988, when they suggested large net terrestrial emissions, Sim-CYCLE also estimated negative ΔNEPs of comparable magnitude (i.e. 0.2 Pg C mo^{-1}). In addition, in 1985, 1989, and 1992, when they suggested net sequestrations, Sim-CYCLE also estimated positive ΔNEPs.

A point-to-point test is desirable and effective in validating the model analysis, at the ecosystem scale. Using the eddy-correlation method, many researchers have measured net ecosystem energy and gas fluxes under various field conditions (e.g. Goulden et al. 1996). They show that the carbon balance of terrestrial ecosystems has a substantial interannual variation greater than 1 Mg C ha^{-1} yr^{-1} (potentially a few Pg C yr^{-1} at the global scale), reflecting the change in habitat weather conditions (Yamamoto et al. 1999). Although a direct comparison was not carried out, we expect that there is a semi-quantitative agreement between these measurements and our model analysis. Another interesting fact is that these flux-oriented studies often suggest that the observed ecosystems are working as a net carbon sink. Including the CO_2 fertilization effect, the Sim-CYCLE simulation also implied a net carbon sequestration into the biosphere (+1.35 Pg C yr^{-1}) of a magnitude comparable to the assumed missing sink.

The Sim-CYCLE analysis could account in part for the anomalously high growth rate of the atmospheric CO_2 concentration after the outbreak of ENSO events (Bacastow 1976, Keeling et al. 1989). Probably, the effect of ENSO events is considerably relevant to the largest ΔNEP in the tropical zone Z3 (see Table 5). For example, after the ENSO episodes in 1983 and 1987, Sim-CYCLE estimated larger carbon emissions from the biosphere (see Fig. 9), and conversely in 1989 after La Niña it estimated larger carbon uptakes, so that the atmospheric CO_2 had corresponding anomalies. However, there remain uncertainties with respect to the effect of ENSO events on ecosystem carbon budget. For example, the Sim-CYCLE analysis does not account for the observed time-lags in the atmospheric CO_2 behind the anomalies in air temperature (Keeling et al. 1989) and in Southern Oscillation Index (Bacastow 1976, Rayner et al. 1999). Because of the time-lag, most of the impacts of the huge ENSO event in 1997 would emerge in 1998, which is not included here. The CO_2 anomaly in relation to the ENSO events would essentially include oceanic processes, such as the interruption of the upwelling of CO_2-rich deep water (Dettinger & Ghil 1998, Feely et al. 1999); the oceanic carbon budget has a variability comparable (SD = 1.0 Pg C yr^{-1}; Joos & Bruno 1998) to the terrestrial one (SD = 1.05 Pg C yr^{-1}, see Table 4). In summary, the terrestrial mechanism had a partial contribution to the observed CO_2 anomaly, but to determine its magnitude will require more information and research.

In relation to the Mt. Pinatubo carbon anomaly, we hypothesize that the large ΔNEP in 1992 (+1.14 Pg C yr^{-1}) was brought about by a series of causal relationships after the Mt. Pinatubo eruption in June 1991 (McCormick et al. 1995, Jones & Kelly 1996, Alados-Alboledas et al. 1997). The estimated ΔNEP in 1992 agrees satisfactorily with the atmospheric CO_2-based value (i.e. +1.0 to 2.5 Pg C yr^{-1} by Keeling et al. 1995), although a contradictory estimation was presented by Francey et al. (1995). We acknowledge indeed that the Mt. Pinatubo carbon anomaly was not a simple phenomenon as hypothesized here, because the oceanic processes might be induced as suggested by Sarmiento (1993). Nevertheless, there are several lines of sound evidence supporting the conclusion that the biospheric processes should make a substantial contribution to the anomaly in the atmospheric CO_2 concentration. For example, Ciais et al. (1995) also estimated a net carbon uptake in the northern middle to high latitudinal ecosystems in 1992 using the SiB2 model, but their estimation (+3.5 Pg C) is much larger than ours (+0.69 Pg C, in Z1 and Z2).

On the role of the terrestrial biosphere in the interannual carbon budget, there are several points demanding further consideration and modification to modelling research, including our analysis. Since Dai & Fung (1993) and Kaduk & Heimann (1994) studied the annual carbon budget of terrestrial ecosystems with empirical models, the issue has attracted the attentions of modelers. For example, Kindermann et al. (1996) applied the Frankfurt Biosphere Model to interannual change from 1980 to 1992, and they found features similar to those described in this paper. However, they ascribed the interannual change in ΔNEP mainly to the change in ΔNPP rather than ΔHR. Myneni et al. (1997) analyzed the temporal change in remotely sensed NDVI (normalized difference vegetation index), and showed that the biospheric carbon budget is sensitive to the interannual change in temperature. They concluded that the warmer climate during recent years has led to a prolonged growing period of vegetation and consequently increased production. Our model analysis is nearly coincident with their satellite-based analysis, e.g. in 1983 negative anomalies were estimated in both observed NDVI and model-based NPP. However, we cannot account for the significantly positive anomalies in NDVI in 1989 to 1990, when Sim-CYCLE estimated only little ΔNPP. Braswell et al. (1997) analyzed the correspondence between ΔNEP and ΔTG, and suggested a response time-lag of approximately 2 yr. Although they attributed the time-lag to an undetermined underground process, we did not find out the nature of the process in this paper, in which responses at the physiological level were mainly addressed. Applying a process-based model (Terrestrial Ecosystem Model), Tian et al. (1998) simulated the carbon budget of the Amazon Basin from 1980 to 1994, and suggested that the regional ΔNEP varied substantially during this period, and that it was sensitive to temperature and soil water change. The model analysis presented in our

paper is one of the few studies that analyzed the interannual time-series of carbon budget anomalies with a mechanistic model and accurate climate dataset.

The climate sensitivity of the biospheric carbon budget may have an important implication with respect to the impact of anticipated global change (IPCC 1996). According to the estimated negative ΔTG-ΔNEP relationship (Fig. 11E), global warming is likely to lead to net release of carbon, i.e. the biotic positive feedback to the prescribed warming, at least in the short term. However, our model analyses revealed that the ΔTG-ΔNEP relationship changes zonally (Table 5) and seasonally (Figs. 12 & 13), and that the precipitation anomaly could play an important role in the carbon budget in northern high and middle latitudinal zones (Table 5). Explicitly, our result suggests that we should develop a finer model and perform a series of sensitivity analyses, so that we are able to quantify the feedback effect. For example, Sim-CYCLE does not yet contain the nutrient dynamics in the soil, which may have a close linkage with carbon dynamics and also be sensitive to temperature (McGuire et al. 1997). In addition, since we focused on the effects of climatic perturbations in this study, the biospheric carbon budget was assumed to be at equilibrium at the beginning of the simulation. Then, the additional human land-use change after 1970 and the carbon emission accompanied with deforestation were not included. In the strong ENSO events in 1983 and 1997, broad areas of tropical forests in Southeast Asia suffered from fire due to drought promoting biomass inflammability. However, we know little about how much carbon was lost from the burned forests, and how much was restored by the following successional regrowth. As Schimel et al. (1997) stated, we should take care that disturbance processes (both natural and anthropogenic) are essential parts of ecosystem dynamics and biogeochemistry, especially when we appraise the biotic feedbacks under future global change. An improved model and simulation result covering a longer term will be presented in our forthcoming research.

Acknowledgements. This study was financially supported, in part, by a Grant-in-Aid from the Ministry of Education, Science and Culture, Japan (10144204 to T.O.), and a Grant-in-Aid of the Research Fellowships of the Japan Society for the Promotion of Science for Young Scientists (to A.I.). The biome dataset was supplied by the United Nations Environment Programme/Global Resource Information Database (UNEP/GRID), Tsukuba, Japan. The climate dataset was supplied by the US National Centers for Environmental Prediction, and the US National Center for Atmospheric Research. We thank Dr R. Weisburd, University of Tsukuba, for his assistance in preparing this manuscript. This paper is dedicated to the late Emeritus Professor M. Monsi, University of Tokyo, who established the dry-matter production theory in plant ecology.

LITERATURE CITED

Alados-Arboledas L, Olmo FJ, Ohvail HO, Teral T, Arak M, Teral K (1997) Evolution of solar radiative effects of Mount Pinatubo at ground level. Tellus 49B:190–198

Amthor JS (1994) Plant respiratory responses to the environmental and their effects on the carbon balance. In: Wilkinson RE (ed) Plant-environment interactions. Marcel Dekker Inc, New York, p 501–554

Bacastow RB (1976) Modulation of atmospheric carbon dioxide by the Southern Oscillation. Nature 261:116–118

Bolin B, Degens ET, Duvigneaud P, Kempe S (1979) The global biogeochemical carbon cycle. In: Bolin B, Degens ET, Kempe S, Ketner P (eds) The global carbon cycle, SCOPE 13. John Wiley & Sons, New York, p 1–53

Braswell BH, Schimel DS, Linder E, Moore B III (1997) The response of global terrestrial ecosystems to interannual temperature variability. Science 278:870–872

Ciais P, Tans PP, Trolier M, White JWC, Francey RJ (1995) A large Northern Hemisphere terrestrial CO_2 sink indicated by the $^{13}C/^{12}C$ ratio of atmospheric CO_2. Science 269: 1098–1102

Collatz GJ, Berry JA, Clark JS (1998) Effects of climate and atmospheric CO_2 partial pressure on the global distribution of C_4 grasses: present, past, and future. Oecologia 114:441–454

Cramer W, Kicklighter DW, Bondeau A, Moore BI, Churkina G, Ruimy A, Scloss A, the Participants of 'Potsdam '95' (1997) Comparing global models of terrestrial net primary productivity (NPP): overview and key results. Potsdam Institute for Climate Impact Research, Potsdam

Curtis PS, Wang X (1998) A meta-analysis of elevated CO_2 effects on woody plant mass, form, and physiology. Oecologia 113:299–313

Dai A, Fung IY (1993) Can climate variability contribute to the 'missing' CO_2 sink? Global Biogeochem Cycles 7:599–609

Dettinger MD, Ghil M (1998) Seasonal and interannual variations of atmospheric CO_2 and climate. Tellus 50B:1–24

Ehleringer J, Björkman O (1977) Quantum yields for CO_2 uptake in C_3 and C_4 plants. Plant Physiol 59:86–90

Ehleringer JR, Cerling TE, Helliker BR (1997) C_4 photosynthesis, atmospheric CO_2, and climate. Oecologia 112: 285–299

Feeley RA, Wanninkhof R, Takahashi T, Tans P (1999) Influence of El Niño on the equatorial Pacific contribution to atmospheric CO_2 accumulation. Nature 398:597–601

Fitter AH, Hay RKM (1981) Environmental physiology of plants. Academic Press, San Diego

Francey RJ, Tans PP, Allison CE, Enting IG, White JWC, Trolier M (1995) Changes in oceanic and terrestrial carbon uptake since 1982. Nature 373:326–330

Gérard JC, Nemry B, François LM, Warnant P (1999) The interannual change of atmospheric CO_2: contribution of subtropical ecosystems? Geophys Res Lett 26:243–246

Goulden ML, Munger JW, Fan SM, Daube BC, Wofsy SC (1996) Exchange of carbon dioxide by a deciduous forest: response to interannual climate variability. Science 271: 1576–1578

Halpert MS, Ropelewski CF (1992) Surface temperature patterns associated with the southern oscillation. J Clim 5:577–593

Houghton RA, Davidson EA, Woodwell GM (1998) Missing sinks, feedbacks, and understanding the role of terrestrial ecosystems in the global carbon balance. Global Biogeochem Cycles 12:25–34

Intergovernmental Panel on Climate Change (IPCC) (1996) Climate change 1995: the science of climate change.

Houghton JT, Filho LGM, Bruce J, Lee H, Callander BA, Haites E, Harris N, Maskell K (eds). Cambridge University Press, Cambridge

Jones HG (1992) Plants and microclimate, 2nd edn. Cambridge University Press, Cambridge

Jones PD, Kelly PM (1996) The effect of tropical explosive volcanic eruptions on surface air temperature. In: Fiocco G, Fua D, Visconti G (eds) The Mount Pinatubo eruption: effects on the atmosphere and climate. Springer, Berlin, p 95–111

Joos F, Bruno M (1998) Long-term variability of the terrestrial and oceanic carbon sinks and the budgets of the carbon isotopes ^{13}C and ^{14}C. Global Biogeochem Cycles 12: 277–295

Joos F, Meyer R, Bruno M, Leuenberger M (1999) The variability in the carbon sinks as reconstructed for the last 1000 years. Geophys Res Lett 26:1437–1440

Kaduk J, Heimann M (1994) The climate sensitivity of the Osnabrück Biosphere Model on the ENSO time scale. Ecol Model 75:239–256

Kalnay E, Kanamitsu M, Kistler R, Collins W, Deaven D, Gandin L, Iredell M, Saha S, White G, Woollen J, Zhu Y, Chelliah M, Ebisuzaki W, Higgins W, Janowiak J, Mo KC, Ropelewski C, Wang J, Leetmaa A, Reynolds R, Jenne R, Joseph D (1996) The NCEP/NCAR 40-year reanalysis project. Bull Am Meteorol Soc 77:437–471

Keeling CD, Bacastow RB, Carter AF, Piper SC, Whorf TP, Heimann M, Mook WG, Roeloffzen H (1989) A three-dimensional model of atmospheric CO_2 transport based on observed winds. 1. Analysis of observational data. Geophys Monogr 55:165–236

Keeling CD, Whorf TP, Wahlen M, van der Plicht J (1995) Interannual extremes in the rate of atmospheric carbon dioxide since 1980. Nature 375:666–670

Kindermann J, Würth G, Kohlmaier GH, Badeck FW (1996) Interannual variation of carbon exchange fluxes in terrestrial ecosystems. Global Biogeochem Cycles 10:737–755

Knorr W, Heimann M (1995) Impact of drought stress and other factors on seasonal land biosphere CO_2 exchange studies through an atmospheric tracer transport model. Tellus 47B:471–489

Kohlmaier GH, Bröhl H, Sire EO, Plöchl M, Revelle R (1987) Modelling stimulation of plants and ecosystem response to present levels of excess atmospheric CO_2. Tellus 39B: 155–170

Kuroiwa S (1966) Dry matter production of plants. In: Kawanabe H (ed) Ecology and evolution. Iwanami Shoten, Tokyo, p 71–100 (in Japanese)

Larcher W (1995) Physiological plant ecology: ecophysiology and stress physiology of functional groups. Springer, Berlin

Leemans R, Cramer WP (1991) The IIASA database for mean monthly values of temperature, precipitation and cloudiness of a global terrestrial grid. IIASA, Laxenburg

Lieth H (1975) Modeling the primary productivity of the world. In: Lieth H, Whittaker RH (eds) Primary productivity of the biosphere. Springer, Berlin, p 237–263

Maisongrande P, Ruimy A, Dedieu G, Saugier B (1995) Monitoring seasonal and interannual variations of gross primary productivity, net primary productivity and net ecosystem productivity using a diagnostic model and remotely-sensed data. Tellus 47B:178–190

Manabe S, Wetherald RT (1987) Large-scale changes of soil wetness induced by an increase in atmospheric carbon dioxide. J Atmos Sci 44:1211–1235

Matthews E (1983) Global vegetation and land use: new high resolution data bases for climate studies. J Clim Appl Meteorol 22:474–487

McCormick MP, Thomason LW, Trepte CR (1995) Atmospheric effects of the Mt Pinatubo eruption. Nature 373: 399–404

McGuire AD, Melillo JM, Kicklighter DW, Pan Y, Xiao X, Helfrich J, Moore B III, Vörösmarty CJ, Schloss AL (1997) Equilibrium responses of global net primary production and carbon storage to doubled atmospheric carbon dioxide: sensitivity to changes in vegetation nitrogen content. Global Biogeochem Cycles 11:173–189

Meentemeyer V (1984) The geography of organic decomposition rates. Ann Assoc Am Geogr 74:551–560

Melillo JM, Prentice IC, Farquhar GD, Schulze ED, Sala OE (1996) Terrestrial biotic responses to environmental change and feedbacks to climate. In: Houghton JT, Meira Filho LG, Callander BA, Harris N, Kattenberg A, Maskell K (eds) Climate change 1995: the science of climate change. Cambridge University Press, Cambridge, p 445–482

Monsi M (1960) Dry-matter reproduction in plants. I. Schemata of dry-matter reproduction. Bot Mag 73:81–90

Monsi M, Saeki T (1953) Über den Lichtfaktor in den Pflanzengesellschaften und seine Bedeutung für die Stoffproduktion. Jpn J Bot 14:22–52

Myneni RB, Keeling CD, Tucker CJ, Asrar G, Nemani RR (1997) Increased plant growth in the northern high latitudes from 1981 to 1991. Nature 386:698–702

New M, Hulme M, Jones P (1999) Representing twentieth-century space-time climate variability. Part 1: development of a 1961–1990 mean monthly terrestrial climatology. J Clim 12:829–856

Oikawa T (1985) Simulation of forest carbon dynamics based on dry-matter production model. 1. Fundamental model structure of a tropical rainforest ecosystem. Bot Mag 98: 225–238

Oikawa T (1995) A simulation study of grassland carbon dynamics as influenced by atmospheric CO_2 concentration. In: Murai S (ed) Toward global planning of sustainable use of the earth: development of global eco-engineering. Elsevier, Amsterdam, p 97–112

Oikawa T (1998) Modeling carbon dynamics of a lucidophyll forest under monsoon climates. Global Environ Res 1: 25–33

Poorter H (1993) Interspecific variation in the growth response of plants to an elevated ambient CO_2 concentration. Vegetatio 104/105:77–97

Potter CS, Klooster S, Brooks V (1999) Interannual variability in terrestrial net primary production: exploration of trends and controls on regional to global scales. Ecosystems 2: 36–48

Raich JW, Schlesinger WH (1992) The global carbon dioxide flux in soil respiration and its relationship to vegetation and climate. Tellus 44B:81–99

Raich JW, Rastetter EB, Melillo JM, Kicklighter DW, Grace AL, Moore B III, Vörösmarty CJ (1991) Potential net primary productivity in South America: application of a global model. Ecol Appl 1:399–429

Rayner PJ, Law RM (1999) The interannual variability of the global carbon cycle. Tellus 51B:210–212

Rayner PJ, Law RM, Dargaville R (1999) The relationship between tropical CO_2 fluxes and the El Niño Southern Oscillation. Geophys Res Lett 26:493–496

Robock A, Mao J (1995) The volcanic signal in surface temperature observations. J Clim 8:1086–1103

Ropelewski CF, Halpert MS (1987) Global and regional precipitation patterns associated with the El Niño/Southern Oscillation. Mon Weather Rev 115:1606–1626

Ruimy A, Jarvis PG, Baldocchi DD, Saugier B (1995) CO_2 fluxes over plant canopies and solar radiation: a review.

Adv Ecol Res 26:1–68
Ryan MG (1991) Effects of climate change on plant respiration. Ecol Appl 1:157–167
Sage RF, Wedin DA, Li M (1999) The biogeography of C_4 photosynthesis: patterns and controlling factors. In: Sage RF, Monson RK (eds) C_4 plant biology. Academic Press, San Diego, p 313–373
Sarmiento JL (1993) Atmospheric CO_2 stalled. Nature 365: 697–698
Schimel DS, VEMAP participants, Braswell BH (1997) Continental scale variability in ecosystem processes: models, data, and the role of disturbance. Ecol Monogr 67:251–271
Teeri JA, Stowe LG (1976) Climatic patterns and the distribution of C_4 grasses in North America. Oecologia 23:1–12
Tian H, Melillo JM, Kicklighter DW, McGuire AD, Helfrich JVKI, Moore BI, Vörösmarty CJ (1998) Effect of interannual climate variability on carbon storage in Amazonian ecosystems. Nature 396:664–667
Whittaker RH (1975) Communities and ecosystems. Macmillan Company, New York
Witcamp M (1966) Decomposition of leaf litter in relation to environment, microflora, and microbial respiration. Ecology 47:194–201
Wittenberg U, Heimann M, Esser G, McGuire AD, Sauf W (1998) On the influence of biomass burning on the seasonal CO_2 signal as observed at monitoring stations. Global Biogeochem Cycle 12:531–544
World Data Centre for Greenhouse Gases (WDCGG) (1998) WMO WDCGG Data Report (WDCGG No. 17). Japan Meteorological Agency, Tokyo
Wullschleger SD, Post WM, King AW (1995) On the potential for a CO_2 fertilization effect in forests: estimates of the biotic growth factor based on 58 controlled-exposure studies. In: Woodwell GM, Mackenzie FT (eds) Biotic feedbacks in the global climatic system: will warming feed the warming? Oxford University Press, Oxford, p 85–107
Yamamoto S, Murayama S, Saigusa N, Kondo H (1999) Seasonal and inter-annual variability of CO_2 flux between a temperate forest and the atmosphere in Japan. Tellus 51B: 402–413
Yokota T, Hagihara A (1996) Seasonal change in the temperature coefficient Q_{10} for respiration of field grown hinoki cypress (*Chamaecyparis obtusa*) trees. J For Res 1: 165–168

Editorial responsibility: Gerd Esser, Gießen, Germany

Submitted: September 21, 1999; Accepted: March 10, 2000
Proofs received from author(s): August 14, 2000